



Forschungszentrum Karlsruhe
in der Helmholtz-Gemeinschaft

Wissenschaftliche Berichte
FZKA 7311

MHD and Corrosion Analysis of Dual Coolant PbLi Blanket Modules for ARIES-CS

C. Mistrangelo

Institut für Kern- und Energietechnik
Programm Kernfusion

Dezember 2007

Forschungszentrum Karlsruhe

in der Helmholtz Gemeinschaft

Wissenschaftliche Berichte

FZKA 7311

MHD and corrosion analysis of Dual Coolant

PbLi blanket modules for ARIES-CS

C. Mistrangelo

Institut für Kern- und Energietechnik
Programm Kernfusion

Forschungszentrum Karlsruhe GmbH, Karlsruhe
2007

Für diesen Bericht behalten wir uns alle Rechte vor

Forschungszentrum Karlsruhe GmbH
Postfach 3640, 76021 Karlsruhe

Mitglied der Hermann von Helmholtz-Gemeinschaft
Deutscher Forschungszentren (HGF)

ISSN 0947-8620

urn:nbn:de:0005-073112

MHD and corrosion analysis of Dual Coolant PbLi blanket modules for ARIES-CS

Abstract

A Dual Coolant Lead Lithium (DCLL) blanket concept has been selected as reference design for the ARIES-CS compact stellarator power plant study. This configuration is characterized by helium cooled first wall and ferritic steel structures, and by a self-cooled breeding zone. Flow channel inserts (FCIs) made of fiber enforced silicon carbide (SiC) composite material are placed in the PbLi channels, serving both as thermal and electrical insulator. The goal is to optimize the Pb-17Li inlet and outlet temperatures for high power cycle efficiency while accommodating the material temperature limits, providing reasonable flow distribution and maintaining an acceptable pressure drop.

In support to this conceptual study of a compact stellarator, a numerical investigation of magnetohydrodynamic (MHD) flows in the poloidal channels that distribute the liquid metal in the breeder units has been carried out to assess the performance of such a concept with regard to the above mentioned goals and constraints. The analysis considers both the electromagnetic coupling of adjacent poloidal ducts and the one that can occur, across the channel insert, between the liquid metal in the bulk and that in the gap formed by the insulating liners and the walls. Moreover, the influence of various parameters such as the electrical conductivity of the SiC insert and the orientation of the magnetic field has been analyzed.

In the second part of this report the problem of the corrosion of the steel wall of poloidal ducts in a DCLL blanket module due to flowing liquid metal is investigated. The mass transfer problem is studied in the gaps formed between the flow channel inserts and the walls. The velocity profile obtained from the MHD analysis has been used as imposed velocity distribution. Results have been obtained considering two different values of the electrical conductivity of the duct insert, i.e. $\sigma_{FCI} = 500 \Omega^{-1}\text{m}^{-1}$ and $\sigma_{FCI} = 100 \Omega^{-1}\text{m}^{-1}$. Larger velocities are present for the highest value of the electrical conductivity of the insert. A first assessment for the concentration of iron inside the gap and for the corrosion rate has been determined.

MHD- und Korrosionsanalyse des Dual Coolant PbLi Blankets für ARIES-CS

Zusammenfassung

Als Referenzdesign eines Fusionsblanket wurde im Rahmen der ARIES – CS Reaktorstudie (Compact Stellarator power plant study) ein so genanntes Dual-Coolant Lead Lithium (DCLL) Blanketkonzept ausgewählt. Dieses basiert auf der Verwendung Helium-gekühlter ferritischer Stahlstrukturen inklusive der ersten Wand und einer selbstgekühlten Blei-Lithium Brutzone. SiC Strömungskanaleinsätze in den PbLi Kanälen isolieren hierbei das Fluid von der Kanalwand sowohl elektrisch als auch thermisch. Ziel der Reaktorstudie ist es, Eintritts- und Austrittstemperaturen im Rahmen der zulässigen Grenztemperaturen der Materialien hinsichtlich eines hohen thermischen Wirkungsgrades zu optimieren und gleichzeitig den magnetohydrodynamischen (MHD) Druckverlust in akzeptablen Grenzen zu halten.

Als Beitrag zur ARIES – CS Reaktorstudie wurden numerische Berechnungen der MHD-Strömungen in den poloidalen Flüssigmetall-Kanälen der Bruteinheiten durchgeführt, um das Verhalten dieses Konzepts hinsichtlich der genannten Ziele und Einschränkungen zu analysieren. Die Berechnungen berücksichtigen sowohl die elektromagnetische Kopplung des Fluids im Spalt zwischen Isolationseinsatz und Stahlstruktur mit dem Fluid im Inneren des Einsatzes, als auch eine Ankopplung benachbarter poloidaler Kanäle. Darüberhinaus wurde der Einfluss zahlreicher Parameter wie der elektrischen Leitfähigkeit von SiC, und der Orientierung des Magnetfeldes auf das Verhalten der MHD-Strömung untersucht.

Im zweiten Teil des Berichtes wird das Problem der Korrosion in poloidalen DCLL-Blanketkanälen untersucht, die dem strömenden Flüssigmetall ausgesetzt sind. Hierzu wird der Stoffübergang von der Stahlwand an das strömende Fluid im Spalt zwischen Isolationseinsatz und Wand analysiert. Hierzu wird das zuvor berechnete Geschwindigkeitsprofil der MHD-Strömung als gegeben vorausgesetzt. Als Beispiele dienen Berechnungen mit zwei verschiedenen elektrischen Leitfähigkeiten der Isolationseinsätze, $\sigma_{FCI} = 500 \Omega^{-1}\text{m}^{-1}$ und $\sigma_{FCI} = 100 \Omega^{-1}\text{m}^{-1}$ wobei sich für höhere Leitfähigkeiten größere Geschwindigkeiten ergeben. Ergebnisse der Rechnungen sind Korrosionsraten an der Wand sowie die Konzentrationsverteilungen von Eisen im Spalt.

Contents

Part I: MHD analysis of DCLL blanket modules for ARIES-CS	1
1 Introduction	1
2 Problem specification	3
2.1 DCLL blanket concept for ARIES-CS	3
2.2 Investigated geometry	5
2.2.1 Effective wall conductance	7
3 Governing equations	8
3.1 MHD pressure drop	9
3.2 Electric flow coupling (multi channel effect)	10
3.3 Flow partitioning among parallel ducts	10
4 Numerical model	11
5 Results	12
5.1 Pure toroidal magnetic field	12
5.1.1 Electric potential and current density	12
5.1.2 Flow distribution	14
5.1.3 Variation of flow channel insert electrical conductivity	15
5.1.4 Pressure drop and flow channel inserts	17
5.2 Inclined magnetic field	19
6 Conclusions	21
7 Future work	22
Part II: Corrosion in poloidal ducts of DCLL blankets	25
1 Introduction	25
2 Formulation of the problem	26
2.1 Geometry	26
2.2 Assumptions	27
2.3 Temperature distribution and heat transfer	27
2.3.1 Heat flow through a multi-layer barrier	28
3 Equations for mass transfer	31
3.1 Boundary conditions	32
3.2 Saturation concentration and diffusion coefficient	34
4 Numerical model	36

5 Results	37
6 Conclusions	40
7 Future investigations	40
References	41

MHD analysis of DCLL blanket modules for ARIES-CS

1 Introduction

The development of nuclear fusion reactors presently focuses on magnetic confinement of the high-temperature plasma by using a toroidal configuration. Tokamaks and stellarators are the most advanced toroidal magnetic confinement concepts.

The tokamak provides the required twist to the magnetic field lines by driving a current through the plasma itself. The combination of various field components produces helical field lines, which wrap around the torus. This reactor configuration requires an array of active control strategies to stabilize the plasma, even under a constant magnetic field.

Stellarators have some important potential operational advantages as fusion power plants. Although they also have a toroidal magnetic field topology, the majority of the confining field is provided by external coils. Therefore, the absence of a net plasma current leads to an inherently steady-state operation with smaller recirculating power and there is no need for continuous power input to the plasma to maintain the magnetic configuration. Plasma control is therefore simplified because the confining fields are controlled with external coils instead of current-drive techniques. The confined plasma is passively stable when a steady magnetic field is applied and therefore stellarators can be operated continuously. Moreover, it has been observed that, even in stellarator experiments with large plasma currents, the external fields stabilize the configuration preventing disruptions. In other words, since current drive power is not needed, the stellarator has a higher plant efficiency and there are no current-drive-related reliability problems.

Besides that, while tokamak configurations have two-dimensional symmetry, stellarators are fully three-dimensional. The extra dimension makes available a wide range of different configurations. Therefore, it might be possible to use this additional degree of freedom to optimize a stellarator in ways that are not possible with tokamaks.

However the three-dimensional nature of the field, the plasma, and the vessel makes much more difficult performing either theory or experimental diagnostics with stellarators and moreover, the helical geometry requires more complex and more sophisticated modules and magnets, and more costly maintenance procedures.

In addition to that, the larger aspect ratio of a stellarator leads to increased size compared to tokamaks. Although the resulting lower power density corresponds to longer component life, the larger dimension, generally dictated by the constraints imposed by the minimum distance between plasma and coils, means more structure and consequently higher cost.

In order to overcome these drawbacks and to increase the attractiveness of the stellarator configuration, approaches that combine the compactness and the moderate aspect ratio of advanced tokamaks with the disruption-free steady state oper-

ation of stellarators have been developed and studied. These concepts are known as Compact Stellarators (CS). The compact stellarator exploits the bootstrap current, namely the self-generated plasma current induced by trapped particles, and three-dimensional plasma shaping to obtain the best features of both stellarators (low recirculating power) and advanced tokamaks (compact size and high power density). Decreasing the plasma aspect ratio should lead to a significant cost reduction. Studies are needed to assess the potential advantages and design issues for compact stellarators as fusion power plants compared to conventional configurations like tokamaks.

The US stellarator community, in its 1998 white paper (Rome (Editor) (1998)), defined a research program with the goal of developing the knowledge about physics features, such as small aspect ratio, use of plasma current, and incorporation of magnetic symmetry in the concept design strategy of stellarator reactors, which could improve the understanding of this configuration. As part of this program, a detailed and integrated study of compact stellarator configurations, called ARIES-CS, was initiated to investigate promising CS power plants and to define key R&D areas (Najmabadi, Raffray, Ku, Lyon and the ARIES Team (2006)). The primary scope of the ARIES-CS reactor study is to develop a more compact machine lowering in this way the costs while preserving the advantages of a stellarator configuration. This project is divided into three phases. The first one focused on selecting a number of blanket concepts and maintenance schemes to be analyzed in detail in the second part of the program. The most promising configuration was used for a complete design analysis in the third phase (Najmabadi and the ARIES Team (2007)).

For the optimization of the stellarator configuration for a power plant, the choice of the breeding blanket plays a fundamental role. A suitable blanket design should assure good performance, reasonable development risk and moderate extrapolation of present knowledge. It should be optimized in order to maximize its heat load capability and thermal efficiency as it has a direct impact on the fusion power and machine size.

Different blanket concepts have been proposed during this conceptual study. After evaluating the pros and cons of various designs a modular Dual Coolant Lead Lithium (DCLL) blanket concept with He-cooled ferritic steel structures and a self-cooled breeding zone containing slowly flowing PbLi has been assumed as a reference design (Najmabadi and Raffray (2006)). In section 2.1 a more detailed description of this concept is given.

In the first part of the present study the MHD flow in six poloidal channels that transport the PbLi in the breeder units is investigated numerically with the purpose to quantify the effects of the interaction of the liquid metal flow with the external magnetic field. Key MHD issues, like flow distribution and pressure losses, are discussed taking into account the electrical flow coupling between the poloidal ducts and the effect of the low but finite electrical conductivity of the flow channel inserts used to electrically and thermally insulate the bulk flow from the steel walls. The flow is studied for the case of a pure toroidal magnetic field (Sect.5.1) and for the

case in which an additional radial component is present (Sect.5.2). Moreover, due to the uncertainties about the value of the electrical conductivity of the silicon carbide insert, different values of this parameter are considered in the following analysis, starting from a very conservative value of $\sigma_{FCI} = 500 \Omega^{-1}\text{m}^{-1}$ and reducing it to $50 \Omega^{-1}\text{m}^{-1}$ (Sect.5.1.3). The obtained results are used to highlight the possible technical problems and to evaluate the feasibility of the present blanket configuration with respect to the afore-mentioned MHD issues.

2 Problem specification

2.1 DCLL blanket concept for ARIES-CS

The Dual Coolant Lead Lithium (DCLL) blanket concept utilizes helium at high pressure and velocity to cool the ferritic steel structures, and slowly moving (10 cm/s or less) Pb-17Li in the self-cooled breeder zone. The first DCLL blanket design was introduced in the EU blanket program around 1992 (Malang, Bojarsky, Bühler, Deckers, Fischer, Norajitra and Reiser (1993)). Insulating coatings were used to reduce the MHD pressure drop (e.g. see Malang and Tillack (1995)). In this concept, the PbLi exit temperature was $\sim 450^\circ\text{C}$ and a thermal efficiency of $\sim 35\%$ was achieved. The DCLL blanket was further developed as part of the ARIES-ST study where insulating flow channel inserts (FCI) were introduced (Tillack and Malang (1997)). The use of insulating liners allowed for a higher PbLi exit temperature ($\sim 700^\circ\text{C}$) leading to an efficiency of $\sim 45\%$. The concept was further evolved as part of the ARIES-CS study, which is the focus of this report, including substantial progress in the areas of flow routing, module attachment, coolant connections, and system integration. The DCLL concept was also chosen as US reference ITER TBM design.

The blanket concepts based on the use of liquid metals have to take into account a number of feasibility issues related to magnetohydrodynamics (MHD) (Morley, Malang and Kirillov (2005)). If the breeding liquid metal flows in direction perpendicular to the applied magnetic field, strong MHD effects occur that lead to an increased pressure drop compared with hydrodynamic flows. This results in larger mechanical stresses and increased pumping power. The interaction between the moving electrically conducting fluid and the confining magnetic field influences the flow distribution and can affect the flow partitioning in parallel ducts. Moreover, the MHD velocity profile may influence the heat transfer between wall and bulk flow as well as tritium permeation due for instance to the occurrence of stagnant zones.

Figure 1 shows an ARIES-CS blanket module and the PbLi flow path inside the distributing poloidal ducts. The liquid metal enters the blanket module through the annular region between two concentric circular pipes, flows upwards in parallel poloidal channels arranged in a row along the first wall (FW). At the top of the breeder unit, according to a two-pass poloidal configuration, the PbLi turns by 180° and moves downwards in a second row of ducts aligned with the back plate (BP). The liquid metal exits the module by flowing through the inner concentric pipe. The

typical size of a blanket module ($2\text{ m tor} \times 2\text{ m pol} \times 0.63\text{ m rad}$) is compatible with a modular replacement through a number of maintenance ports using articulated booms.

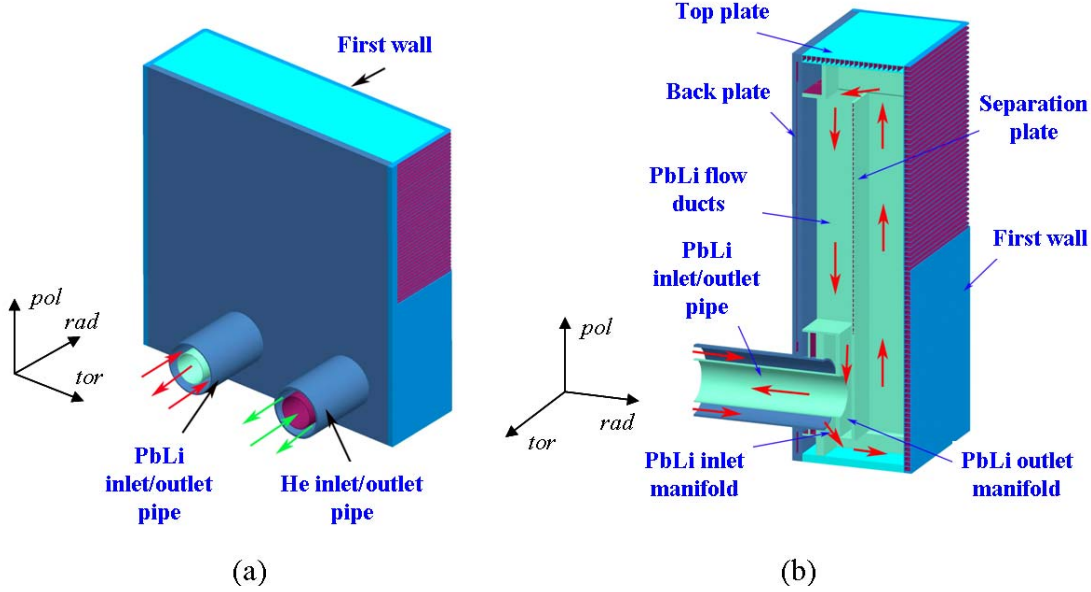


Figure 1: (a) Blanket module. (b) Liquid metal flow path in poloidal ducts.

In order to minimize the MHD pressure drop to those in insulating channels (see Sect.3.1), in the present DCLL blanket design flow channel inserts (FCIs) made of silicon carbide composite material with low electrical conductivity are arranged inside the poloidal channels to electrically insulate the breeding zone from the walls. The inserts decouple electrically the PbLi flow from the steel walls by interrupting the current paths towards the conducting walls. Moreover, since the inserts have a low thermal conductivity, they act also as thermal insulation. This allows for high operation temperature, i.e. increased thermal efficiency, while accommodating the constraints related to the maximum allowable surface temperature of steel. Hence, the temperature at the fluid-wall interface is maintained below the compatibility limit. On the other hand, the use of FCIs carries a higher development risk mostly due to SiC_f/SiC material development.

Figure 2 shows the typical arrangement of the flow channel insert in a poloidal duct. These inserts have no structural function. They are loosely fitted into the poloidal channels, and close to the duct walls there are narrow gaps filled with liquid metal. These latter are connected to the bulk region by a small slot that extends along the entire poloidal length of the liner. The main purpose of this opening and of the gap, as pointed out by Malang 2006 (private communication), is to minimize the primary stresses on the insert and to avoid strong mechanical interaction between the liners and the wall. Moreover, in that way the fabrication and insertion of these insulating components do not require too high precision. The gap should be as small as possible since the heat produced in the liquid metal passes into the helium coolant

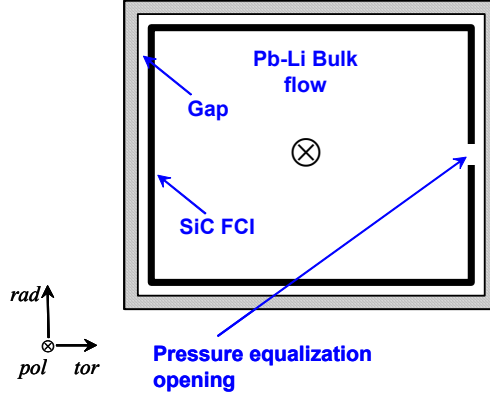


Figure 2: Cross-section of a poloidal duct with silicon carbide (SiC) flow channel insert (FCI). This latter has an opening that connects gap and bulk flow allowing to equalize the pressure in these two fluid domains to minimize the primary stresses on the insert.

in the walls. This results in reduced efficiency of the power conversion cycle.

Another important aspect that has to be considered is the wall-material losses into the liquid metal due to corrosion. This latter should be controlled and maintained within acceptable values.

2.2 Investigated geometry

Figure 3a shows a partial view of the liquid metal path inside the poloidal ducts. By cutting this assembly by means of the $rad - tor$ plane marked by the dashed line and indicated section A-A, the schematic cross-section displayed in Fig.3b is obtained. This represents the geometry used for the present numerical study where six poloidal channels have been considered.

The geometric features, the dimensions and the material properties are chosen according to the last review of the reference blanket design for ARIES-CS (Raffray, El-Guebaly, Ihli, Malang, Najmabadi, Wang and the ARIES-CS Team (2007)) as displayed in Fig.4. Here the dimensions of the gap and the slot are enlarged to show better the details of the geometry. In the figures the insulating inserts lining the internal surface of the ducts are indicated by solid bold lines. The channel cross-section is almost square ($24.5 \text{ cm (tor)} \times 25 \text{ cm (rad)}$) and the gap between the FCI ($t_{FCI} = 5 \text{ mm}$) and the wall is very small ($t_{gap} = 1 \text{ mm}$) compared with the width of the central region of the ducts ($2L = 23.3 \text{ cm}$). In the present study it is assumed that the poloidal ducts are long enough to assure that in most part of the channels fully developed flow conditions are established.

The six poloidal channels have common electrically conducting walls (grid plates and separation plate) through which an exchange of currents is possible. This leads to an electrical coupling of adjacent fluid domains. This phenomenon, known as multichannel effect, may influence the velocity distribution, the pressure drop and flow partitioning in the ducts. We observe that in this geometry the poloidal ducts

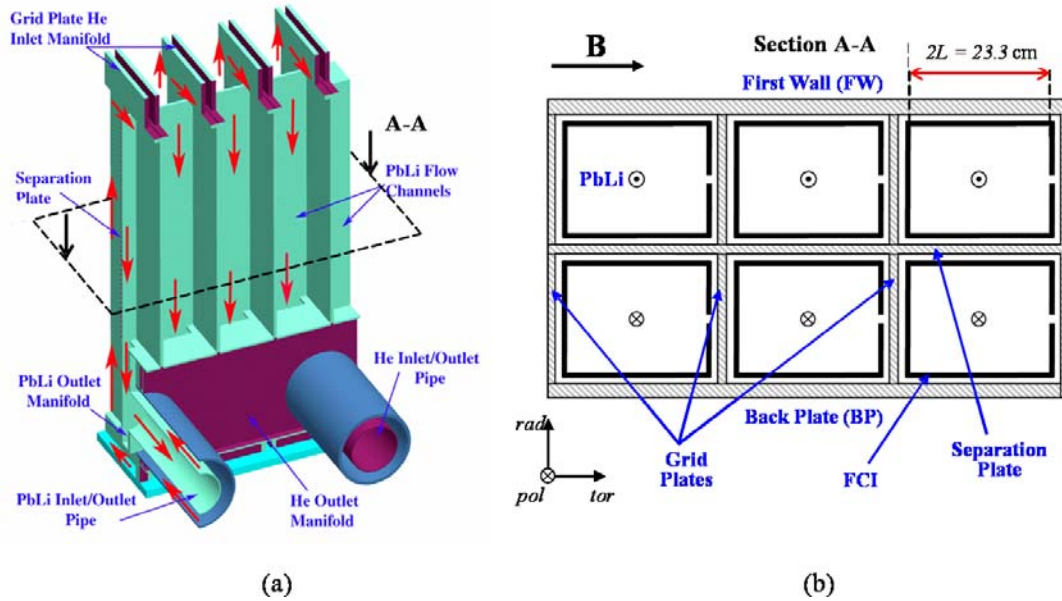


Figure 3: (a) Partial view of PbLi flow path in poloidal channels. (b) Cross-section of six poloidal ducts as considered in the numerical analysis. The solid bold line indicates the flow channel inserts.

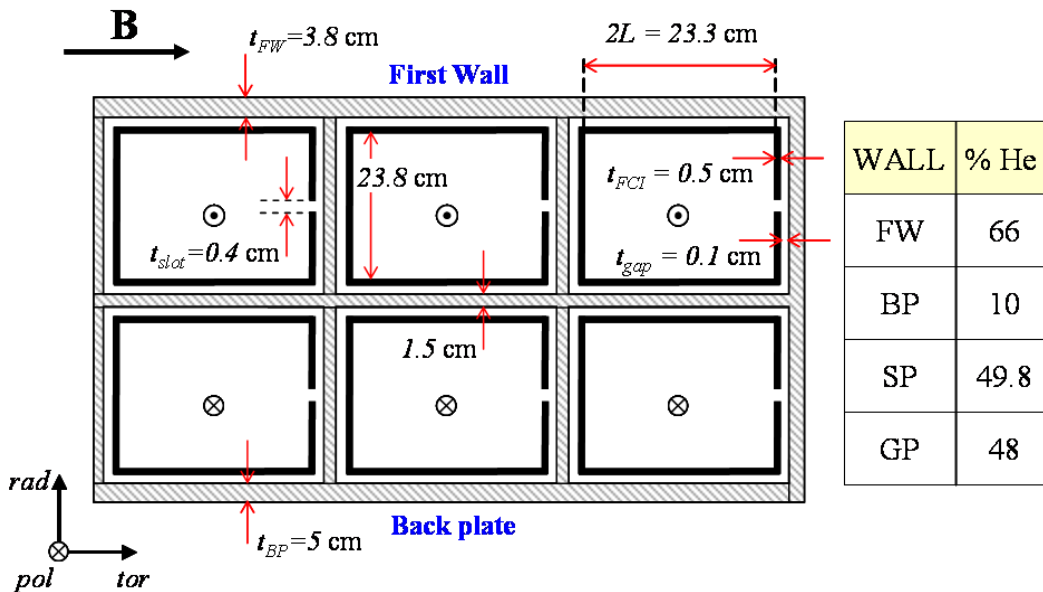


Figure 4: Sketch of the investigated geometry with the dimensions given by the design. The table on the right summarizes the volume fraction of helium in the walls (FW=first wall, BP=back plate, SP=separation plate, GP=grid plate).

are arranged in such a way that channels with co-current flow are electrically coupled through the grid plates. Moreover, they are aligned in a row along the toroidal direction. This row is then coupled radially with counter-current flow domains through the separation plate. The global flow structure is the result of toroidal and radial electrical coupling, taking into account that the inserts should reduce the intensity of the coupling.

As mentioned before, primary mechanical stresses in the FCI are minimized by connecting the outer gap and the inner flow region by means of a slot made for equalizing the pressure in the two subdomains. Preliminary numerical analyses have been performed to understand the effects of the presence of this opening on the flow distribution in the channel. Considering a pure toroidal magnetic field, aligned with the channel walls (first wall, back plate, separation plate), the slot can be positioned either close to the walls parallel to the magnetic field, called side walls, or on the portions near walls perpendicular to the field, named Hartmann walls. Calculations for the case with the opening at the side wall show that at this location it would cause a local strong reversed flow due to the presence inside the slot of current paths perpendicular to the applied magnetic field (Fig.5). These results are in agreement with the ones available in literature (Smolentsev, Morley and Abdou (2006)). For this reason, in the present study, the pressure equalization opening has been positioned at the Hartmann walls.

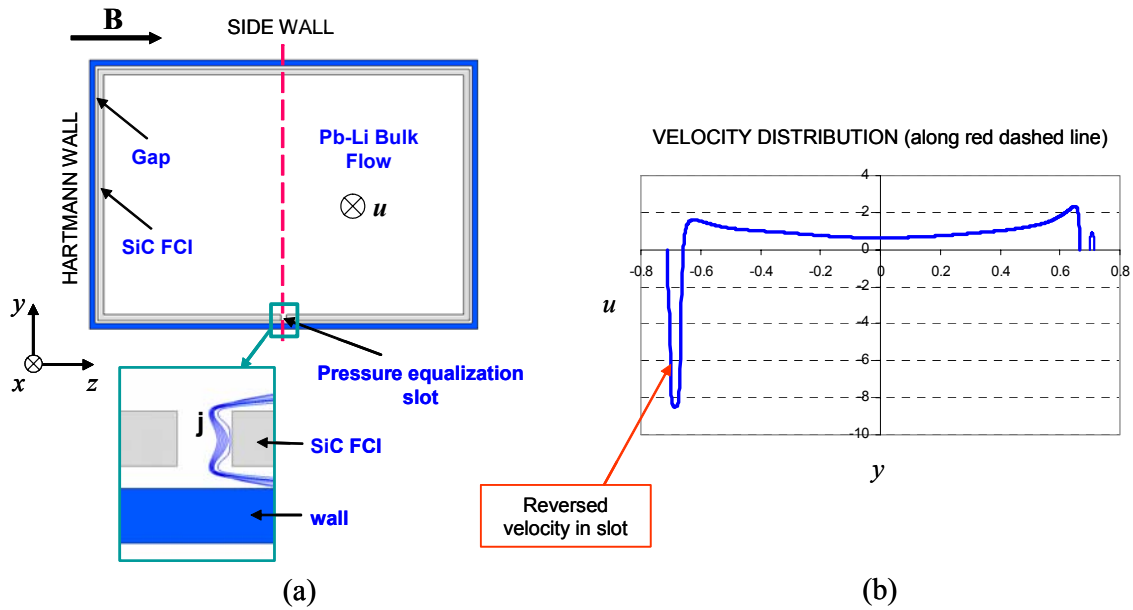


Figure 5: (a) Cross section of a poloidal duct with flow channel insert. The detailed view shows the current distribution through the pressure equalisation slot. (b) As a result of the presence of currents perpendicular to the magnetic field, a strong locally reversed flow occurs in the opening.

2.2.1 Effective wall conductance

Since each wall contains helium cooling channels, their real thickness has been reduced for the numerical MHD analysis depending on the volume of helium flowing in the ducts. An effective wall thickness $t_{w,\text{eff}}$ has been defined as

$$t_{w,\text{eff}} = t_w(1 - \varepsilon), \quad (1)$$

in which ε is the volume fraction of helium in the considered wall. The values of ε for the different walls are summarized in the table in Fig.4. In that way, an effective electrical conductance c_{eff} comparable to the real one c is obtained:

$$c = \frac{\sigma_w t_w}{\sigma L} \implies c_{\text{eff}} = \frac{\sigma_w t_{w,\text{eff}}}{\sigma L}, \quad (2)$$

where σ_w and σ are the electrical conductivity of the wall and fluid material, respectively, t_w is the thickness of the wall and L is the characteristic length for the geometry under study corresponding to half toroidal width of one duct (see Fig.3b). The conductance parameter c describes the ratio of the electric conductance of the wall to the fluid one.

3 Governing equations

The equations describing the steady state laminar, incompressible, viscous, MHD flow are written in dimensionless form so that the relative importance of the different terms can be inferred by the size of multiplying non-dimensional groups, whose magnitudes give an idea of the relative strength of the various forces acting on the flow. These dimensionless equations consist of conservation of momentum, mass and charge and Ohm's law (Shercliff (1965), Müller and Bühler (2001)):

$$\frac{1}{N} (\mathbf{v} \cdot \nabla) \mathbf{v} = -\nabla p + \frac{1}{Ha^2} \nabla^2 \mathbf{v} + \mathbf{j} \times \mathbf{B}, \quad (3)$$

$$\nabla \cdot \mathbf{v} = 0, \quad (4)$$

$$\nabla \cdot \mathbf{j} = 0, \quad (5)$$

$$\mathbf{j} = -\nabla \phi + \mathbf{v} \times \mathbf{B}. \quad (6)$$

By combining equations (5) and (6) a Poisson equation for the electric potential is obtained:

$$\nabla^2 \phi = \nabla \cdot (\mathbf{v} \times \mathbf{B}). \quad (7)$$

In these equations the variables \mathbf{v} , p , \mathbf{j} , \mathbf{B} and ϕ denote the velocity, the pressure, the current density, the magnetic field and the electric potential scaled by the

reference quantities v_0 , $\sigma v_0 B_0^2 L$, $\sigma v_0 B_0$, B_0 and $v_0 B_0 L$, respectively. Here, the half width of the channel, measured along the toroidal direction, is chosen as characteristic length L ($L = 11.65$ cm) and the average velocity in a particular cross-section of the duct is taken as the velocity scale v_0 . The quantity B_0 is the magnitude of the imposed magnetic field. The fluid properties, namely the density ρ , the electrical conductivity σ and the kinematic viscosity ν are assumed to be constant.

By assuming a small magnetic Reynolds number ($Re_m \ll 1$), the main effect of the interaction between the electromagnetic field and the moving fluid is associated with the appearance of the electromagnetic force $\mathbf{j} \times \mathbf{B}$, which is the source term in the momentum equation. This is the so called inductionless approximation since, under these conditions, the magnetic field induced by currents in the fluid is negligible compared to the external one (Walker (1986)). This means that the magnetic field is not affected by the flow. Hydrodynamic equations and Maxwell's equations are therefore coupled by the electromagnetic Lorentz force and the induced electric field $\mathbf{v} \times \mathbf{B}$ present in Ohm's law.

In eq. (3) two non-dimensional groups, the Hartmann number Ha and the interaction parameter N , are present:

$$Ha = B_0 L \sqrt{\frac{\sigma}{\rho \nu}}, \quad N = \frac{\sigma L B_0^2}{\rho v_0}. \quad (8)$$

The square of the Hartmann number characterizes the ratio of electromagnetic forces to viscous forces while the interaction parameter represents the ratio of electromagnetic forces to inertia forces.

In the present study the channels have conducting walls with electrical conductivity σ_w . Moreover, the inserts have a certain conductivity $\sigma_{FCI} > 0$. Therefore part of the current flowing in the fluid may close its path through the FCIs and the walls and the following equations have to be solved in the solid domains:

$$\mathbf{j}_s = -\frac{\sigma_s}{\sigma} \nabla \phi_s, \quad \nabla \cdot \mathbf{j}_s = 0, \quad (9)$$

where the subscript s stands for solid domains like the walls ($\sigma_s = \sigma_w$) or the flow channel inserts ($\sigma_s = \sigma_{FCI}$).

As boundary condition at all fluid-solid interfaces the no-slip condition is applied

$$\mathbf{v} = 0.$$

The electric boundary conditions at the fluid-solid interface state the continuity of wall-normal component of current density and electric potential

$$j_n = j_{ns}, \quad \phi = \phi_s.$$

The normal component of the electric current density vanishes at the external surface of the wall because the surrounding medium is assumed to be insulating.

3.1 MHD pressure drop

As mentioned before, the increased pressure drop due to MHD effects represents a feasibility issue for the DCLL blanket concept. Since the MHD pressure drop depends

on the magnitude of the total current induced in the fluid, it can be mitigated by decoupling the conducting walls from the electric circuit that controls the core current density. This can be obtained by using insulating flow channel inserts that prevent the current path from closing inside the electrically conducting duct walls leading to a lower induced current.

In electrically insulated ducts the currents have to close within the fluid via the thin Hartmann layers. This results in lower pressure drop than in ducts with electrically conducting walls. In order to show the importance of the flow channel insert as technical and design solution for the DCLL blanket concept, in the following the difference between the pressure distribution in electrically conducting ducts and the one in insulating channels is presented.

In the general case the MHD pressure gradient for strong magnetic fields can be expressed as

$$p = -(\rho\nu v_0/L^2)kHa^2, \quad (10)$$

where $k(Ha, N, c, \dots)$ stands for a pressure drop coefficient that may depend on all the parameters affecting the flow like the magnetic field, represented by the Hartmann number Ha , inertial forces, given by the interaction parameter N , and wall conductivity, expressed by the conductance ratio c . The term in bracket, $\rho\nu v_0/L^2$, is the laminar viscous hydrodynamic pressure scale. The formula (10) shows that the MHD pressure drop exceeds the hydrodynamic one by a factor kHa^2 .

For fusion relevant conditions ($Ha^{-1} \ll c \ll 1$) we have $k \approx c$ in conducting channels, i.e. the pressure gradient is proportional to the square of the Hartmann number. Instead in insulating channels $k \approx Ha^{-1}$ and the pressure gradient scales only linearly with the applied magnetic field (Ha),

$$p = -(\rho\nu v_0/L^2)Ha. \quad (11)$$

Therefore, providing adequate insulation in the poloidal channels allows reducing the MHD pressure drop according to the previous formulas.

3.2 Electric flow coupling (multi channel effect)

Poloidal channels have common electrically conducting walls across which leakage currents may flow that are responsible for electromagnetic coupling of adjacent flow domains. This phenomenon is known as multi channel effect (McCarthy and Abdou (1991), Molokov (1993)). The exchange of currents and electric power affects the velocity distribution in parallel ducts influencing in this way the pressure drop and flow partitioning as well. The presence of the FCI should minimize or reduce this coupling.

3.3 Flow partitioning among parallel ducts

When the pressure drop along multiple ducts is forced to be the same, for instance due to the fact that the channels are fed by a common manifold or pipe system, as in the DCLL blanket design, the flow rate in each duct is in general different from that in neighboring channels. This difference has to be evaluated in order to check if

the fluid distributes homogeneously and uniformly among the parallel poloidal ducts. A proper arrangements of the channels forming the assembly may lead to a weak electric flow coupling that mitigate the flow rate imbalance in the ducts.

4 Numerical model

The present investigation is carried out using the commercial package CFX-5.6, which is based on the finite volume method and on a modified form of the SIMPLE algorithm for pressure-velocity coupling to ensure mass conservation (Patankar (1980)). The discrete system of linearized equations is solved by an iterative procedure.

Since magnetohydrodynamic equations are not available as option in CFX-5, these equations have been implemented in the code by means of Fortran subroutines. In order to describe MHD flows it is necessary to introduce the Lorentz force as a body force in the momentum equation and to solve a Poisson equation (7) for the electric potential. The implementation of MHD equations in CFX has been described by Mistrangelo (2005).

Another aspect that has to be carefully considered in CFD simulations is the mesh used to discretize the computational domain. It is important to resolve properly the geometric features that affect the flow and the regions where the largest gradients of the variables occur, such as the boundary layers that develop along the walls. By increasing the magnetic field strength, namely the Hartmann number, the thickness of the boundary layers decreases. The size of those at walls parallel to the magnetic field varies as $\delta_{side} \sim Ha^{-1/2}$, while the thickness of the boundary layers along walls perpendicular to the imposed field scales as $\delta_{Ha} \sim Ha^{-1}$. Therefore the need of resolving adequately these layers, while preserving the mesh quality, leads to a progressive rise in the total number of nodes in the computational domain with increasing Hartmann number. As a consequence, restrictions on the accuracy of the solution at high Hartmann numbers are related to limitations in the memory storage and computer capabilities.

In the geometry under study, the liquid metal flows both in the internal large domains, surrounded by the flow channel inserts, almost electrically insulated from the external conducting walls, and in the small gaps between the inserts and the steel walls, where a strong reduction of the velocity is expected. In all the fluid domains viscous boundary layers develop along the walls and the FCIs, and their thickness varies depending on their orientation with respect to the magnetic field. These boundary layers match the solutions in the bulk region with the no-slip condition at the walls and along the inserts. In order to obtain an accurate and reliable solution, all these boundary layers have to be resolved adequately.

The convergence of the solution is judged both considering the value of the residuals of velocity and mass conservation and by monitoring the solution variables in fixed points in the computational domain during the run. Values of interest are for instance the maximum velocity in the parallel layers and the potential difference between the side walls. The calculations of MHD flows are stopped when all the root mean square residuals are equal or less than 10^{-5} and the variables at the monitored locations remain constant.

5 Results

The results presented first in this section for a pure toroidal magnetic field are obtained for the most conservative case that has been analyzed with a relatively high value of the electrical conductivity of the flow channel inserts, $\sigma_{FCI} = 500 \Omega^{-1}\text{m}^{-1}$. This case is presented in detail since it is useful to know the effects of poor insulating properties of the insert related for instance to a partial deterioration of insulation during operation.

The influence of the electrical conductivity of the inserts has also been investigated since it may vary depending on the techniques used for fabricating the fiber enforced SiC composite material. In the last section, results for an inclined magnetic field, namely for the case when a radial component of the confining field is present, are described.

5.1 Pure toroidal magnetic field

5.1.1 Electric potential and current density

Let us consider first the distribution of electric potential ϕ in the six poloidal ducts.

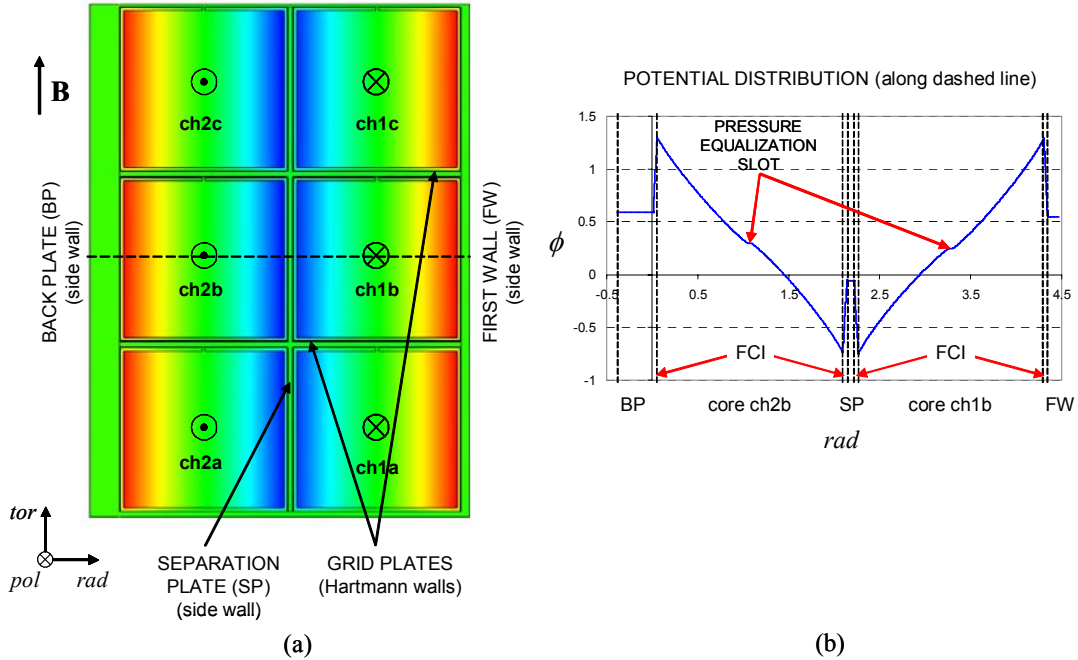


Figure 6: (a) Contour plot of the electric potential in the cross-section of the poloidal ducts. (b) The potential is plotted in radial direction along the dashed line passing through the central ducts, connecting the back plate and the first wall.

Figure 6a displays the contour plot for the electric potential in the various fluid domains. In Fig.6b the potential is plotted along the radial direction, namely along a

line connecting the back plate (BP) to the first wall (FW), in the middle of the central ducts, as indicated by the dashed line. In this diagram the potential in the gaps is not visible due to their small size. The electric potential is nearly constant through the walls and strong gradients occur across the flow channel inserts. The amount of current that flows tangentially inside the insert is negligible compared with that crossing it. In the center of the ducts the potential distribution is locally deformed. The inflection points are caused by the presence of the pressure equalization slots in the inserts. The discontinuity in the electrical conductivity, represented by the opening, leads to the development of an internal parallel layers that spread into the fluid along magnetic field lines. Therefore this distortion in the potential profile propagates along the entire magnetic field line that passes through the slot linking the Hartmann wall and the opposite side of the insert. The uniform electric potential in the separation plate indicates that there is no exchange of currents across this wall. This observation is confirmed by the analysis of the current distribution in the assembly. It shows the presence of singular points, produced by the current vector field, located at the intersections between the separation plate and the grid plates. Figure 7c indicates how the currents coming radially from the grid plates redistribute tangentially in toroidal direction along the separation wall.

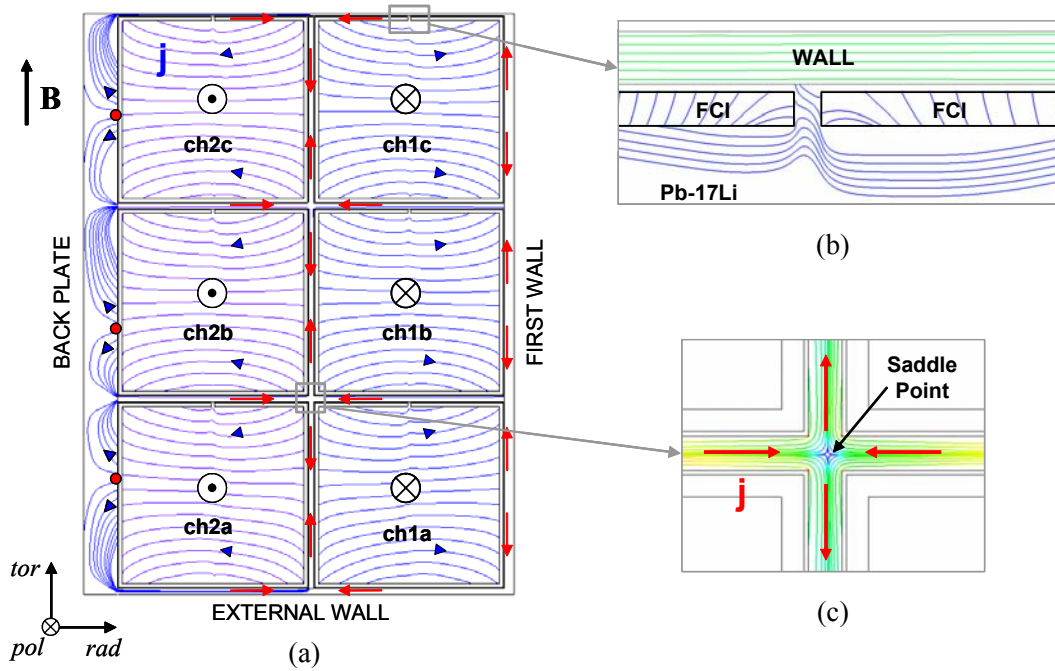


Figure 7: Current streamlines showing (b) the deformation due to the presence of the slot and (c) the saddle point that indicates the distribution of currents from radial to toroidal direction in the separation plate.

FCIs do not carry a significant amount of current in tangential direction compared to that which flows within the adjacent thin Hartmann layers that form in the inner large duct at walls perpendicular to the magnetic field. The currents flow preferentially in these thin boundary layers instead of entering the flow channel insert,

choosing the path of lower electric resistance. The currents that pass through the insert move into the highly conducting region behind it, namely in the narrow liquid metal gap and in the walls.

Another interesting characteristic of the current distribution is the local deformation of the streamlines caused by the pressure equalization opening (Fig.7b). This deformation is present in the whole parallel internal layer that develops in the fluid along magnetic field lines.

From this analysis of electric potential and current distribution it is possible to conclude that, as a result of the presence of the inserts and the particular arrangement of the ducts, the resulting electric coupling is weak and a rather uniform partition of the flow in the parallel poloidal ducts is expected.

5.1.2 Flow distribution

Figure 8a shows the contour plot of velocity in the cross-section of the geometry. In Fig.8b the non-dimensional velocity is plotted as a function of the radial coordinate along the dashed line in the middle of the central ducts, in the domain enclosed by the insert. The velocity distribution indicates that the presence of the internal layer, which develops from the pressure equalization slot, determines a local velocity deficit in the center of the ducts observable along the entire field lines crossing the opening. For the high value of the electrical conductivity of the insert considered in the present analysis ($\sigma_{FCI} = 500 \Omega^{-1}\text{m}^{-1}$) the velocity in this zone changes even the direction and the flow is locally reversed.

The increased velocity along the FCIs at walls parallel to the magnetic field is related to the imperfect insulating properties of Hartmann walls. The side walls do not affect strongly the flow since, due to the presence of the insert, they behave as being almost insulating. This is confirmed by the fact that, in the absence of the insulating barrier the electrically conducting side walls would lead to the formation of velocity jets with a higher maximum value close to the common internal wall (SP) and the velocity profile would exhibit a parabolic distribution along magnetic field lines. In this case instead the maximum velocity at the insert is comparable at each side wall and this rise of the velocity can be regarded as a deformation of the core flow (Bühler and Molokov (1994)). In the case of sufficiently high σ_{FCI} the jet velocity exceeds substantially the average bulk velocity. A detailed numerical study has been further performed showing that increasing the size of the slot leads to an enlargement in radial direction of the region where the velocity deficit occurs.

Considering now the velocity distribution in the gaps formed between the inserts and the separation plate (Fig.8c), it can be observed that the velocity profile is almost parabolic and the maximum velocity is less than half of that in the internal ducts. In the gaps near the back and the first wall a similar velocity distribution is found.

In the gaps formed between the Hartmann walls, perpendicular to the magnetic field, and the inserts, at some distance from the pressure equalization opening, the velocity distribution has the characteristics of the classic Hartmann flow with uniform core velocity and thin boundary layers with strong velocity gradients. Analogously, in the internal ducts the velocity profile along magnetic field lines is characterized by a constant core value and thin viscous boundary layers near the inserts, where

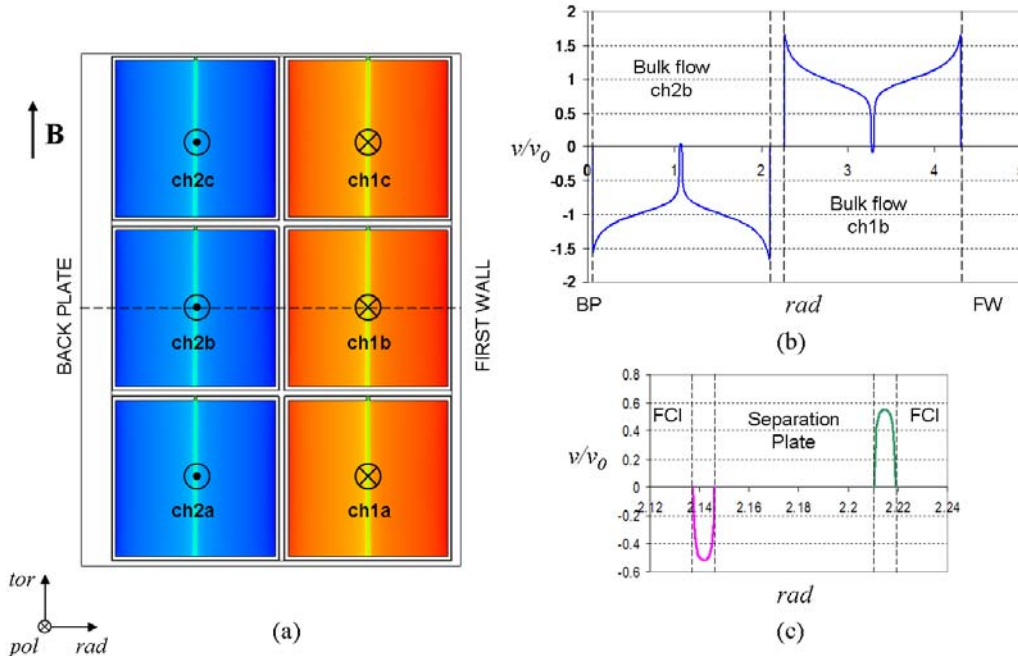


Figure 8: (a) Contour plot of velocity in the assembly cross-section. The non-dimensional velocity is plotted along the radial direction (b) in the central internal ducts, and (c) in the side gaps formed between separation plate (SP) and inserts, for $Ha = 5000$ and $\sigma_{FCI} = 500 \Omega^{-1}\text{m}^{-1}$.

the velocity decays exponentially to satisfy the no-slip condition. In the core the velocity is only a function of the radial coordinate.

This can be seen in Fig.9b where the dimensionless velocity is plotted as a function of the toroidal direction along the three lines A, B, C displayed in Fig.9a. The velocity profile along the line C, which marks the position of the internal parallel layer caused by the discontinuity in the electrical conductivity of the wall, shows the already mentioned local reduction of the velocity. For this large value of σ_{FCI} a zone where the flow is reversed compared to the core stream appears. Approaching the slot the velocity reduces and the fluid turns in the main flow direction.

5.1.3 Variation of flow channel insert electrical conductivity

By comparing the results obtained for various values of the electrical conductivity of the flow channel inserts it is observed that, with decreasing the conductivity σ_{FCI} , the velocity reduces in all external subdomains, namely in the gaps. This is shown in Fig.10b where the non-dimensional velocity in the side gaps adjacent to the separation plate is plotted along the radial direction for various σ_{FCI} . A similar effect on the velocity profile is observed in the gaps close to the back plate and the first wall. In the inner duct cores instead the flow tends towards a more uniform distribution: the velocity deficit in the internal parallel layer is attenuated and the increased velocity at side walls reduces (Fig.10a).

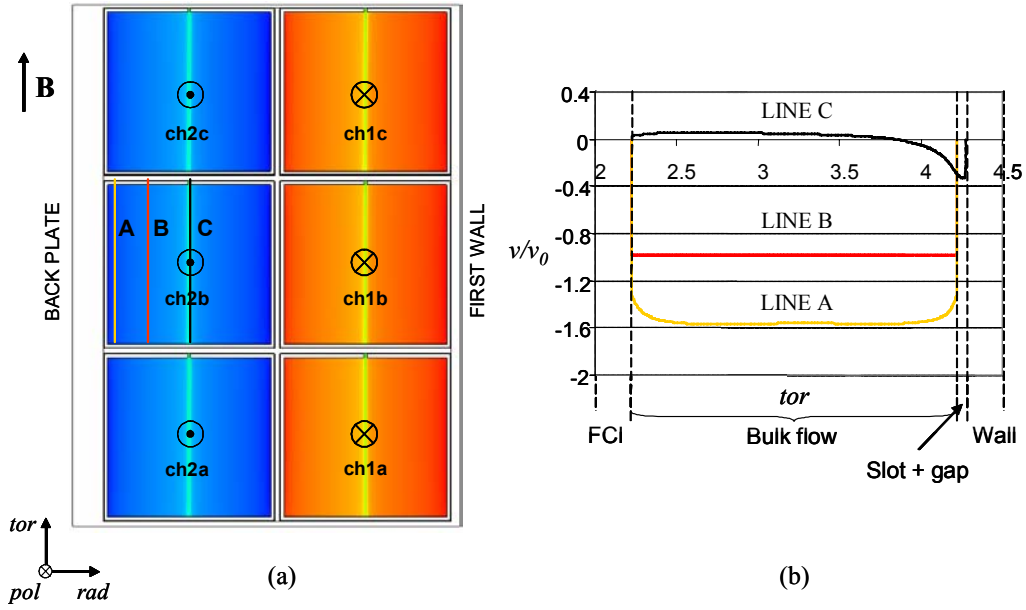


Figure 9: (a) Contour plot of the velocity in the cross-section of the geometry . (b) Non-dimensional velocity plotted along the toroidal direction in the central duct ch2b, for $Ha = 5000$ and $\sigma_{FCI} = 500 \Omega^{-1}m^{-1}$. The velocity profile along the line C shows the local velocity deficit in the internal parallel layer. For this high value of σ_{FCI} the flow is even reversed compared to the main core stream.

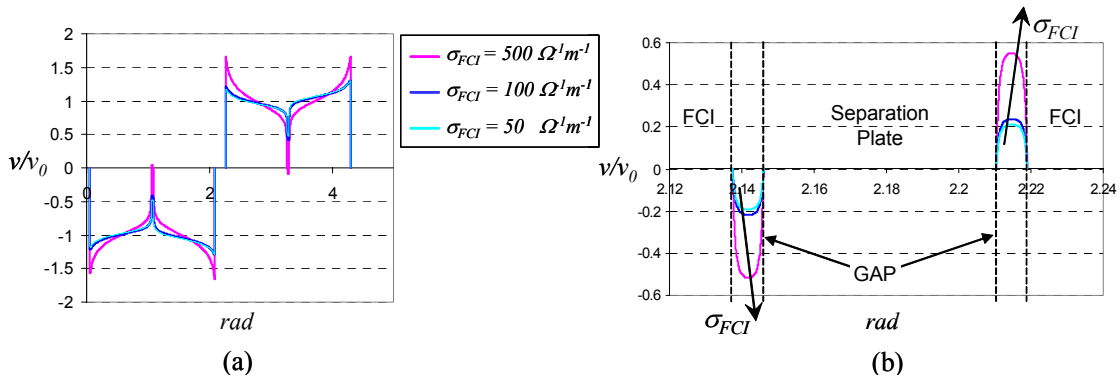


Figure 10: Non-dimensional velocity plotted along the radial direction (a) in the large inner fluid domains delimited by the FCIs, and (b) in the side gaps formed between separation plate and inserts, for $Ha = 5000$ and various σ_{FCI} .

It is interesting to notice that the changes of the velocity profile by reducing the electrical conductivity of the insert from $\sigma_{FCI} = 100 \Omega^{-1}\text{m}^{-1}$ to $\sigma_{FCI} = 50 \Omega^{-1}\text{m}^{-1}$ are quite modest. This can indicate that the insulating properties of the FCI are already sufficiently good, so that a further reduction of their electrical conductivity will not seriously affect the flow anymore at this Hartmann number.

Let us consider now the velocity distribution in toroidal direction, namely along the applied magnetic field lines, for different values of the electrical conductivity of the flow channel insert σ_{FCI} . In the inner ducts the velocity near the side walls, parallel to \mathbf{B} , at a fixed radial location (line A in Fig.11), reduces with decreasing σ_{FCI} . In the internal parallel layer the local deficit of the velocity is progressively attenuated with a reduction of the difference between this local minimum and the average bulk velocity. Moreover, the reversed flow disappears (velocity profile along line C in Fig.11).

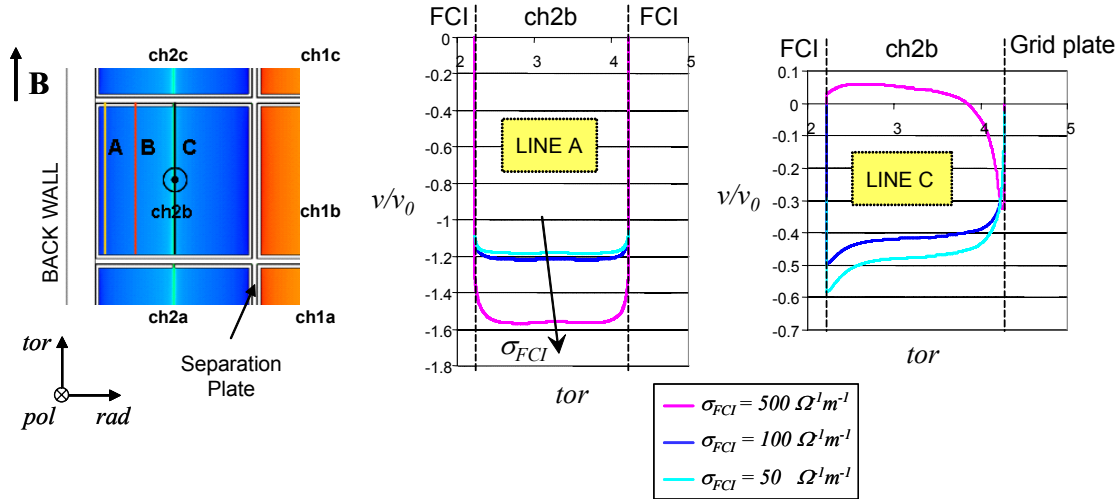


Figure 11: Non-dimensional velocity in the internal duct, delimited by the FCI, plotted along the toroidal direction at various radial positions (line A and line C), for $Ha = 5000$ and different values of σ_{FCI} .

Figure 12 displays the flow distribution in the gaps at Hartmann walls. At some distance from the pressure equalization slot, the velocity distribution has the characteristics of the classical Hartmann flow with uniform core velocity and thin boundary layers with strong velocity gradients. By decreasing the electrical conductivity of the insert the core velocity reduces.

5.1.4 Pressure drop and flow channel inserts

As stated before, for the design of liquid metal blankets the knowledge of the pressure drop due to MHD phenomena is a fundamental requirement. Keeping the overall system at sufficiently low pressure is necessary both for safety and for mechanical reasons. An excessively high pressure drop causes an increase in the required pumping power and strong mechanical loads.

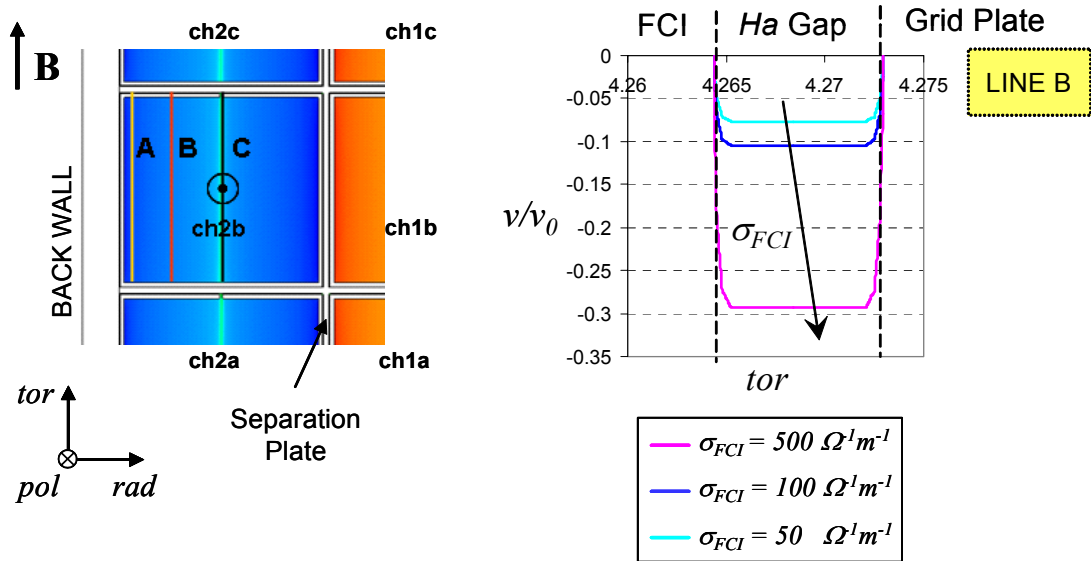


Figure 12: Non-dimensional velocity in the Hartmann gap, close to wall perpendicular to the magnetic field, plotted along the toroidal direction (line B), for $Ha = 5000$ and different values of σ_{FCI} .

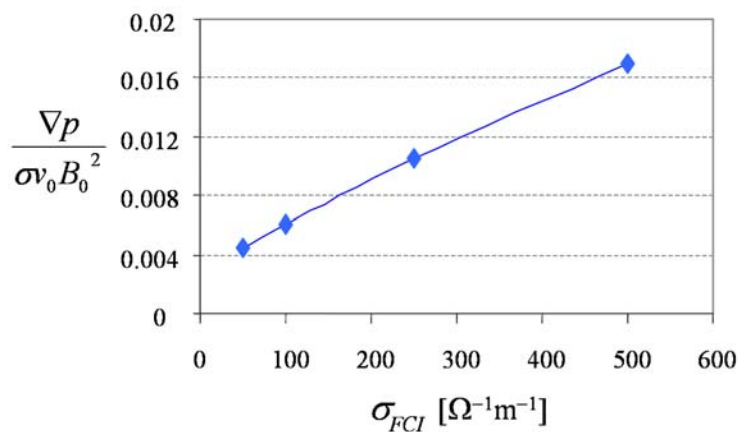


Figure 13: Non-dimensional pressure gradient as a function of the flow channel insert electric conductivity σ_{FCI} , for $Ha = 5000$.

In Fig.13 the dimensionless pressure gradient is plotted as a function of the electrical conductivity σ_{FCI} of the insert. According to the described geometry and the PbLi physical properties (Jauch, Karcher, Schulz and Haase (1986)) the value of the magnetic field corresponding to $Ha = 5000$, as used for the numerical analysis, is about 1.6 T. Assuming an average velocity of 0.1 m s^{-1} , a pressure loss of $\Delta p = 1.1 \cdot 10^{-3} \text{ MPa m}^{-1}$ for $\sigma_{FCI} = 100 \text{ } \Omega^{-1} \text{ m}^{-1}$ is found.

The value of the magnetic field for which MHD flows have been investigated is lower than the one in real applications. This is related to the limited available computational resources and, as a consequences, to the maximum number of points that can be used to discretize the computational domain. This implies that boundary and internal layers can be properly resolved only up to a maximum Hartmann number. Nevertheless, studies for moderate Hartmann numbers lead to scaling laws that allow to extrapolate the results to higher magnetic fields.

5.2 Inclined magnetic field

Magnetic fields in stellarators are quite complex and exhibit in general, in addition to the main toroidal field B_{tor} , also radial B_{rad} and poloidal B_{pol} components. For that reason a slightly inclined magnetic field with $B_{rad} \neq 0$ has been considered. The results discussed here are obtained for $B_{rad} = 10\% B_{tor}$, $\sigma_{FCI} = 500 \text{ } \Omega^{-1} \text{ m}^{-1}$ and $Ha = 5000$.

The solutions for the electric potential and the velocity are inclined along magnetic field lines. In Fig.14 the contour plots of the electric potential are displayed to highlight this inclination according to the magnetic field orientation. The velocity distribution shows the presence of internal layers that spread into the fluid from the duct corners and from the location of the pressure equalization slot, developing parallel to the magnetic field lines. Previously, for the case of a pure toroidal magnetic field, the maximum velocity was localized near the center of the side walls (parallel to \mathbf{B}). Now it is shifted towards one of the duct corners close to the lateral toroidal walls, as indicated by the crosses in Fig.14.

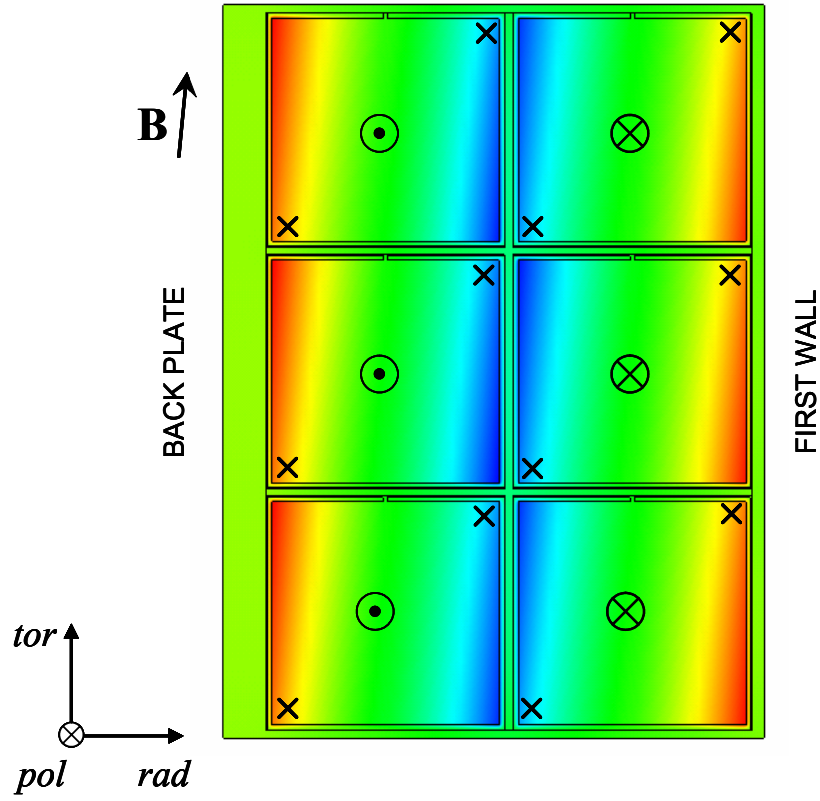


Figure 14: Contour plot of the electric potential for $\sigma_{FCI} = 500 \Omega^{-1}\text{m}^{-1}$, $Ha = 5000$ and $B_{rad} = 10\% B_{tor}$. The crosses indicates the position of the maximum velocity in each fluid domain.

6 Conclusions

The fully developed MHD flow in six poloidal channels of a DCLL blanket, selected as a reference design for the compact stellarator ARIES-CS, has been investigated numerically for a fixed Hartmann number $Ha = 5000$. Results are given for velocity, current, potential distribution and for pressure drop, considering the full electrical coupling between adjacent fluid domains and the influence of the electrical conductivity of the flow channel inserts. These latter are used to electrically and thermally insulate the ducts. The geometric features are taken according to the last review of the DCLL blanket design for ARIES-CS.

The flow is studied both in the case of a pure toroidal magnetic field and in the case of an inclined field. The latter situation corresponds to the presence of a radial component of the imposed magnetic field.

When a toroidal magnetic field, namely a field parallel to the back plate, first wall and separation plate, is considered, the velocity profile in the radial direction, inside the inner large ducts is characterized by higher values along the side walls of the flow channel inserts. This rise of the velocity is due to the imperfect insulation of the Hartmann walls due to the finite conductivity of the insert material. The fact that the velocity distribution in radial direction does not show a strong asymmetry, even if the side walls have different conductance, may indicate that these walls behave as being almost insulating even for the most conservative case with $\sigma_{FCI} = 500 \Omega^{-1}\text{m}^{-1}$. Therefore the flow distribution is only slightly influenced by the characteristics of the lateral walls (back plate, separation and first wall), but it is mainly governed by the properties of flow channel inserts at the Hartmann walls perpendicular to \mathbf{B} . Owing to a discontinuity in the electrical conductivity of the wall represented by the pressure equalization slots, internal layers develop along magnetic field lines in which the velocity is reduced. This velocity deficit may lead to a local increase of the temperature that has to be taken into account. Moreover, for sufficiently high σ_{FCI} the flow in the internal layer may even be reversed compared to the main stream. Across the side gaps between the insulating inserts and the separation plate, the velocity profile is almost parabolic. Along magnetic field lines the velocity distribution, at some distance from the internal layer, resembles that of a classical Hartmann flow with uniform core velocity and thin boundary layers with strong velocity gradients.

The electric potential and current density distributions highlight the absence of current exchange across the separation plate. This indicates that the particular arrangement of the poloidal channels, characterized by co-current flow in ducts coupled at Hartmann walls (grid plates) and counter-current flow in the ones joined at the side wall (separation plate), and the use of the insulating liners lead to a weak electric coupling and a quite uniform partitioning of the flow in the ducts.

Concerning the MHD pressure drop in the poloidal channels, it has been verified that, even in the most conservative case with relatively high electrical conductivity of the insulating barriers, the pressure losses caused by 2D currents are small and acceptable.

If the Hartmann number is increased, the layers become thinner but it is expected

that, by improving the insulation quality according to the rise of the magnetic field, a similar flow distribution remains and the scaling laws will be still valid.

Considering the possibility of tailoring the properties of the flow channel insert material by controlling the manufacturing process, we investigated the effects of the electrical conductivity of the liner on the features of the MHD flow in the poloidal ducts. The reduction of the electrical conductivity of FCI leads to a decrease of the velocity at side walls, a more uniform core flow distribution and a mitigation of the velocity deficit in the internal parallel layer. Analogously, in the side and Hartmann gaps there is a progressive reduction of the velocity. For sufficiently small values of the insert electrical conductivity the flow in the Hartmann gaps can be regarded as almost stagnant. Such a slow velocity may give rise to concerns about an increased permeation of tritium to the helium cooling channels, but reduces the risk of strong corrosion of steel walls.

The results for an inclined magnetic field ($B_{rad} \neq 0$) show that the solutions for velocity and potential are inclined and aligned with the imposed field. The maximum velocity, located in the middle of the side layers for the case with $B_{rad} = 0$, is now shifted towards one of the corners of the lateral toroidal walls.

Considering the described characteristics of the MHD multichannel flow, a quite positive picture of the possible performance of the present arrangement of poloidal channels in the selected blanket design is conveyed even for a conservative value of the electrical conductivity of the inserts. The MHD flow coupling between the parallel poloidal ducts is very weak. Nevertheless, it is necessary to keep in mind that a major issue for this blanket concept is represented by the possibility of constructing proper insulating barriers and producing insert materials with suitable properties. Moreover, as suggested in the following section, further problems have to be considered and analyzed to get a complete picture of MHD phenomena and to understand their importance in determining the performance of the DCLL blanket for the ARIES-CS. Particularly relevant are the contribution to the MHD pressure drop of 3D flows occurring e.g. in manifolds, expansions and concentric pipes, the uncertainties on the gap size and over the precise value of the electrical conductivity of the inserts during the lifetime of a blanket.

7 Future work

Three-dimensional calculations should be performed to predict the pressure drop in more complex 3D geometries. For instance in the region where the fluid expands from the feeding circular pipe into the poloidal ducts, in transition zones of varying magnetic field or in the 180° turn at the top of the blanket module. In these zones strong 3D MHD phenomena are expected, that can cause high pressure losses. While for fully developed 2D flows insulating inserts reduce efficiently the MHD pressure drop, these barriers cannot improve the situation for 3D cases, where the currents find a closure inside the fluid along 3D paths. The prediction of these 3D current flows, which can have a great influence on flow distribution especially in insulated ducts, requires additional theoretical and experimental work.

Considering the poloidal length of the channels, the inserts will be likely divided in various pieces overlapping at some point along the axis of the duct. The MHD flow in these zones may be important to analyze and its effects should also be taken into account in the pressure drop assessment. Moreover, the inserts are placed loosely in the channels and a precise defined gap, constant over the entire poloidal length seems very difficult to realize. Therefore, the study of the influence of the size of the gap can represent a further interesting topic.

In the case of toroidal magnetic field it could be useful to verify also the validity of the assumption of laminar flow. The presence of instabilities in the side layers cannot be excluded. They would lead to the appearance of vortices with axes aligned with the magnetic field, which therefore are not too strongly damped by the field.

Corrosion in poloidal ducts of DCLL blankets

1 Introduction

The corrosion behavior of ferritic steel exposed to flowing PbLi is an issue for the feasibility of liquid metal blanket concepts. Therefore, one of the concerns for the DCLL blanket design is the compatibility of the moving PbLi with the steel structures. Material losses should be maintained within acceptable limits. This implies the need of fixing criteria to limit these losses over the whole lifetime of a blanket module. Such a criterion could be given in terms of reduction of wall thickness, e.g. the limit could correspond to a maximum percentage of local wall thickness.

Some experimental studies for corrosion of steel due to flowing liquid metal exist whereas a limited number of theoretical analyses is available (see e.g. Malang (1984)). It has been found that ferritic or martensitic steel corrosion in PbLi is characterized by a homogeneous dissolution without the formation of a superficial corrosion layer and the intensity of this phenomenon is closely related to the temperature and to the hydrodynamics of the liquid metal flow (Broc, Flament, Fauvet and Sannier (1988), Flament, Tortorelli, Coen and Borgstedt (1992)). Corrosion tests have shown that the corrosion rate of martensitic steels is strongly dependent on the PbLi velocity, suggesting that the process is controlled by the diffusion of dissolved elements in the laminar sub-layer (Sannier, Flamment and Terlain (1991)).

The concentration of dissolved elements, the diffusion coefficient and the material properties of liquid metal depend on the temperature, and the material losses are determined, among other factors, by the local fluid-wall interface temperature. Therefore, in order to perform a numerical corrosion analysis, it is necessary to estimate the temperature distribution in the geometry under study. In section 2.3 a quite detailed description of the procedure used to evaluate the temperature field is given.

The saturation values for the concentration of iron in the eutectic alloy PbLi, required as boundary condition at the wall-fluid interface, and the mass diffusion coefficient have been calculated from relations reported in literature (Sect.3.2). It should be noted that there are still uncertainties on the accuracy of these formulas due to the large scattering of published data, often obtained from experiments performed even under very different conditions. In particular, most of the experiments have been performed in the turbulent regime. Therefore, it is not always easy to compare the results or to extrapolate them to the desired range of temperature required for the calculations. Moreover, the purpose of the present study is to obtain a first assessment for the concentration of iron in PbLi and for corrosion rate. For that reason, several assumptions have been made to simplify the problem.

2 Formulation of the problem

2.1 Geometry

Figure 15 shows the geometry used for the numerical analysis described in this second part of the report. The flow in the gap between the flow channel insert (FCI) and the separation plate (SP) has been considered and the problem of mass transfer of corrosion products from the ferritic steel wall into the fluid has been investigated.

The calculations have been carried out starting from the MHD velocity distribution in the middle of a side gap at the wall parallel to the magnetic field, since this is the location where the highest gap velocity is observed. Therefore these flow conditions should represent the limiting case that produces the largest corrosion rate.

The gap has a width $L = 0.001$ m and the total poloidal length, considering the two-pass configuration, is equal to 4 m.

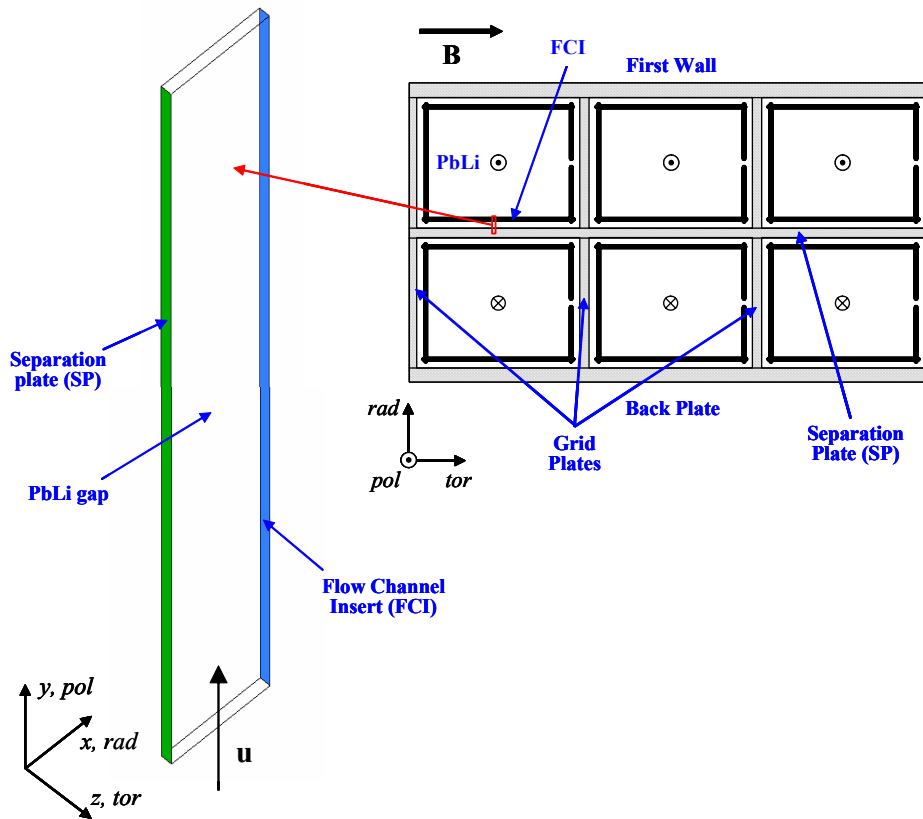


Figure 15: Geometry used for the numerical study of the corrosion problem. Thin slice through the side gap located between the flow channel insert (FCI) and the separation plate (SP).

2.2 Assumptions

A fixed fully developed MHD velocity distribution obtained from previous calculations has been imposed in all the computational domain.

In order to simplify the mass transfer problem and to get a first estimation of the corrosion rate in the poloidal gaps in the channels forming a DCLL blanket module, some assumptions have been considered and applied to the problem.

It is assumed that the heat transfer is steady state, namely the quantity of heat flowing from one point to another by unit time is constant and the temperatures at each point in the system do not change with time. Moreover, for simplicity, the volumetric heat generations in the FCI and PbLi are not considered in this initial model. They would tend to increase the liquid metal temperature in the gap, and should be included in more detailed models.

It has been assumed that the temperature in the bulk flow increases linearly along the poloidal direction. This is equivalent to assume that, since the FCI is almost insulating from the thermal point of view, heat losses from the fluid into the gap through the liner are small. The temperature at the FCI surface, facing the internal large duct, is set equal to the value in the liquid metal core flow. In addition to that, since the temperature gradient through the gap, i.e. the difference between the temperature at the steel wall and the one at the FCI is quite small (see Sect.2.3.1), in the calculations it has been assumed that the material properties of PbLi are constant across the gap but they can change poloidally along the flow path. Since the gap is quite thin, the thermal conductivity of PbLi is high and the velocity is small, it is assumed also that the temperature in the gap is governed by heat conduction.

2.3 Temperature distribution and heat transfer

In order to calculate the temperature field in the gap, required for evaluating the saturation concentration at the wall and the diffusivity that depend on the temperature distribution, it is necessary to consider the heat transfer process in the geometry under study.

The equation used to express the heat conduction through a wall is known as Fourier's law. Under steady conditions where there is a linear temperature distribution, for a one dimensional plane wall it can be written as:

$$\dot{Q} = \lambda A \frac{\Delta T}{\Delta x}, \quad (12)$$

where \dot{Q} [W] is the heat transferred per unit time, λ [$Wm^{-1}K^{-1}$] is the thermal conductivity of the material, A [m^2] the heat transfer area, ΔT [K] the temperature difference across the material and Δx [m] the thickness of the considered layer.

Equation (12) can be rearranged as:

$$\dot{Q} = A \frac{\Delta T}{\Delta x / \lambda}. \quad (13)$$

The inverse of the thermal conductivity, $1/\lambda$, is called thermal resistivity and by multiplying it by the thickness of the wall we obtain the thermal resistance R of the barrier

$$R = \frac{\Delta x}{\lambda}. \quad (14)$$

The transfer of thermal energy between a surface and a moving fluid occurs instead due to convection. This process is described by the following equation:

$$\dot{Q} = hA\Delta T = A \frac{\Delta T}{1/h},$$

where h [$Wm^{-2}K^{-1}$] is the heat transfer coefficient and ΔT is the temperature difference between the surface and the bulk fluid. The inverse of the heat transfer coefficient $1/h$ is the thermal resistance (in our case the resistance due to convection in helium).

2.3.1 Heat flow through a multi-layer barrier

The heat transfer through the helium ducts, the channel walls, the liquid metal gap, the flow channel insert and the PbLi bulk flow can be seen as a multi-layer heat transfer problem (see Fig.16).

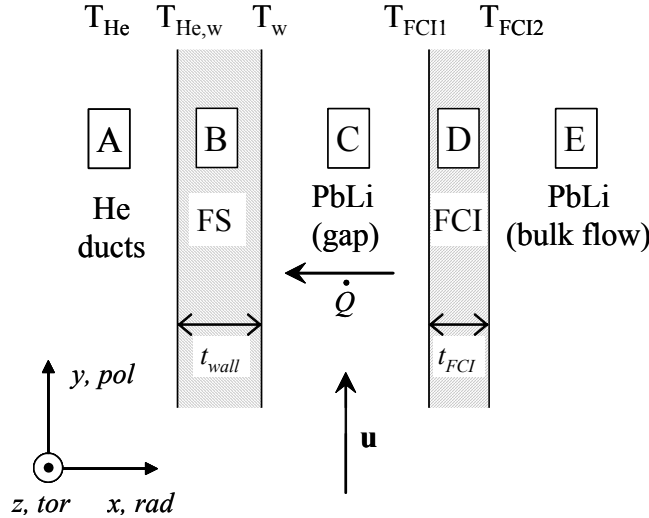


Figure 16: The investigated geometry consists of different regions: A indicates the helium cooling ducts, B is the ferritic steel wall, C is the liquid metal gap, D the flow channel insert and E the PbLi bulk flow. \dot{Q} is the heat flux through the multi-layer barrier.

Each layer constitutes a resistance R_i to heat flow. Therefore, one can give an overall thermal resistance R_{tot} for the multi-layer barrier as:

$$R_{tot} = \sum R_i. \quad (15)$$

In the specific problem under investigation the overall thermal resistance is given by:

$$R_{tot} = \frac{1}{h_{He}} + \frac{t_{wall}}{\lambda_{FS}} + \frac{t_{gap}}{\lambda_{PbLi}} + \frac{t_{FCI}}{\lambda_{SiC}}, \quad (16)$$

where h_{He} is the helium heat transfer coefficient, t_{wall} , t_{gap} and t_{FCI} are the thickness of the wall, the width of the gap and the size of the flow channel insert, respectively. The thermal conductivities of ferritic steel, PbLi and SiC composite are indicated by λ_{FS} , λ_{PbLi} and λ_{FCI} . The general heat transfer formula becomes:

$$\dot{Q} = A \frac{\Delta T}{R_{tot}} = A \frac{(T_{FCI2} - T_{He})}{R_{tot}}. \quad (17)$$

Where T_{FCI2} and T_{He} (Fig.16) are the temperatures at the FCI-liquid metal bulk flow interface and the one of the helium, respectively. As a first approximation it is assumed that T_{FCI2} coincides with the temperature in the core flow. The temperature distribution can be calculated considering that the heat flux remains constant through all the layers, and assuming that the heat transfer area A is constant. The procedure followed to determine the temperature field is summarized in Table 1.

\dot{Q}	$A \frac{(T_{FCI2} - T_{He})}{R_{tot}}$	
<i>Helium</i>	$A h_{He} (T_{He,w} - T_{He})$	$\implies T_{He,w}$
<i>Wall</i>	$A \frac{\lambda_{wall}}{t_{wall}} (T_w - T_{He,w})$	$\implies T_w$
<i>PbLi gap</i>	$A \frac{\lambda_{PbLi}}{t_{gap}} (T_{FCI1} - T_w)$	$\implies T_{FCI1}$

Table 1: Procedure to calculate the temperature distribution in the computational domain, knowing the temperature profile in the liquid metal bulk flow (T_{FCI2}) and that of helium in cooling ducts (T_{He}). T_{FCI1} denotes the temperature of the PbLi-FCI interface, which faces the gap.

It can be observed that the thermal conductivity of the liquid metal is a function of the temperature:

$$\lambda_{PbLi}(T_{PbLi}) = 1.95 (1 + 0.0101 T_{PbLi}), \quad (18)$$

therefore in order to calculate the transferred heat \dot{Q} , required to estimate the temperature field, a suitable guess for the outlet temperature of the liquid metal in the gap has to be found. This temperature has been calculated by means of an easy iterative procedure, knowing the outlet temperature of helium T_{He} and the one of the liquid metal in the bulk flow T_{FCI2} . Figure 17 shows the temperatures at the outlet of the duct in the steel wall, in the liquid metal gap and across the flow channel insert. In that way we can refine our guess till reaching a final value $T_{gap,out} = 746$ K. This temperature has been assumed as the wall-fluid interface temperature $T_{w,out}$.

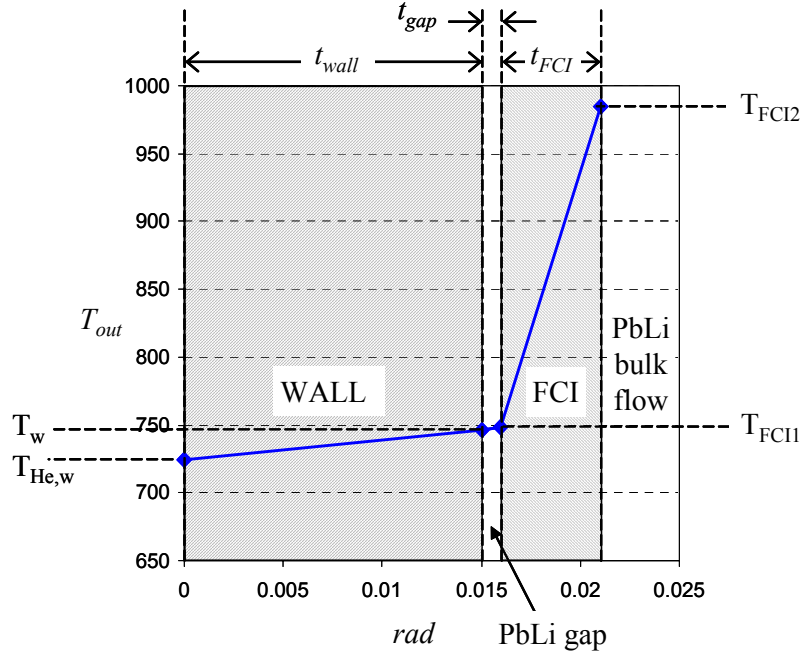


Figure 17: Temperature distribution at the outlet of the poloidal duct across the steel wall, the liquid metal gap and the FCI. In the temperature names the subscript "out" has been omitted to simplify the notation.

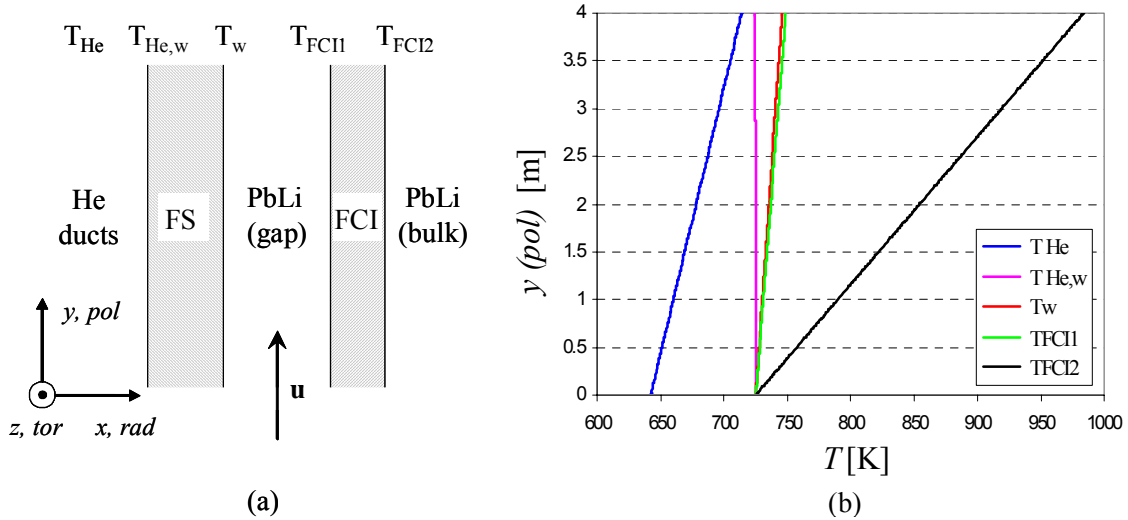


Figure 18: (a) Scheme of the considered geometry: He ducts, steel wall, PbLi gap, FCI and bulk flow. (b) Temperature distribution along the poloidal direction. T_{He} is the temperature of helium, $T_{He,w}$ the value at the He-wall interface, T_w at the wall-PbLi gap interface, T_{FCI1} and T_{FCI2} the values on the two sides of the insert.

This assumption is justified by the fact that the variation of temperature across the gap width is very small.

Figure 18b shows the temperature distribution obtained by the described procedure. The difference between the temperature at the wall and the one at the insert is quite small as shown in Fig.19. The maximum difference, which occurs at the outlet, is lower than 3 K.

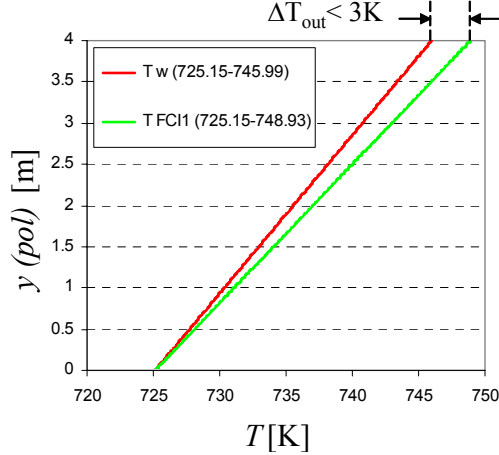


Figure 19: Temperature distribution along the poloidal direction. T_w is the temperature at the wall-fluid interface in the gap and T_{FCI1} is the one at the fluid-FCI interface, facing the gap. The maximum temperature difference occurs at the outlet and it is $\Delta T_{out} < 3K$.

3 Equations for mass transfer

Mass transfer process is the result of transporting material from a solid surface to the bulk of a flowing fluid and the driving force is the difference in the concentration of dissolved elements. The global transport is given by diffusion and bulk convection. In order to calculate the transport of a corrosion product, present in the liquid metal in a certain concentration c_i , where i denotes the considered species i.e. the dissolved element, a convection-diffusion equation is used:

$$\frac{\partial c_i}{\partial t} + (\mathbf{v} \cdot \nabla) c_i = \nabla \cdot (D_i \nabla c_i) \quad (19)$$

where \mathbf{v} is the velocity of PbLi obtained from the analysis of the MHD flow (Sect.5, part I) and $D_i(T)$ is the mass diffusion coefficient or mass diffusivity of the solute i in the liquid metal that is a function of the temperature.

This equation can be written in dimensionless form by assuming a characteristic velocity v_0 , chosen as the average velocity in a poloidal duct ($v_0 = 4 \text{ cm s}^{-1}$), and a typical length L , taken here as the width of the gap ($L = 0.001 \text{ m}$). For a steady

state problem the non-dimensional equation reads as:

$$(\mathbf{v} \cdot \nabla) c_i = \nabla \cdot \left(\frac{D_i}{v_0 L} \nabla c_i \right) = \nabla \cdot \left(\frac{1}{Pe} \nabla c_i \right), \quad (20)$$

where Pe is the Peclet number that depends on the temperature through the diffusion coefficient $D(T)$. The Peclet number is the ratio of the solute convected by the fluid to the amount transported by diffusion. In other words, it relates the rate of advection of a flow to its rate of diffusion, giving a measure of the relative importance of these two processes. It is given by the product of the Reynolds number Re with the Schmidt number Sc . This latter describes the ratio of momentum diffusivity (expressed by the kinematic viscosity ν) and mass diffusivity:

$$Pe = Re Sc = \frac{v_0 L}{\nu} \frac{\nu}{D} = \frac{v_0 L}{D}. \quad (21)$$

Physically the Schmidt number relates the thickness of the hydrodynamic laminar layer δ_h and the one of the mass-transfer boundary layer δ_d . The higher the value of Sc , the thinner will be the diffusion layer and the faster will be its formation. For liquid metals, where $\nu \gg D$, the Schmidt number is very high indicating that the mass diffusion layer δ_d is submerged under the hydraulic boundary layer δ_h ($\delta_d \ll \delta_h$).

The mass flux of the solute i from the channel wall into the bulk of the fluid is given by:

$$j_i = k_i (c_i^w - c_i^b), \quad (22)$$

where k_i is the mass transfer coefficient for the dissolved relevant species i and it depends only on the flow conditions, c_i^w is the concentration of the solute at the wall and c_i^b is the concentration in the bulk of the fluid or the average concentration in the cross-section. If $c_i^w > c_i^b$ the mass flux is directed from the wall into the fluid. The mass flux can be also expressed as

$$j_i = -D_i \frac{\partial c_i}{\partial n}, \quad (23)$$

where n is the coordinate normal to the steel wall (radial direction x in Fig.15).

3.1 Boundary conditions

For solving the present problem a fixed velocity profile has been imposed as obtained from the investigation of the MHD flow in poloidal ducts of a DCLL blanket (Sect.5, part I).

Figure 20 summarizes the boundary conditions for the temperature and the concentration that have been used for the numerical study.

At the inlet a constant value of temperature has been considered, $T_{in} = 452$ °C and the concentration has been set at the saturation value at the entrance temperature, $c_0 = c_{sat}(T_{in})$.

At the interface between the separation plate and the liquid metal flowing in the gap the wall temperature distribution has been given as calculated considering the heat transfer across the multi-layer barrier formed by helium channels, wall,

gap and insulating insert (see Sect.2.3). For this dissolution process, the surface concentration distribution has been assumed equal to the saturation values at the temperature of the wall $c_w = c_{sat}(T_w)$ (He, Li and Mineev (2001)). The expression used to obtain such values is regarded as a possible option but uncertainties are still present (Sect.3.2) and ongoing discussions could lead in future to modifications of the considered formula.

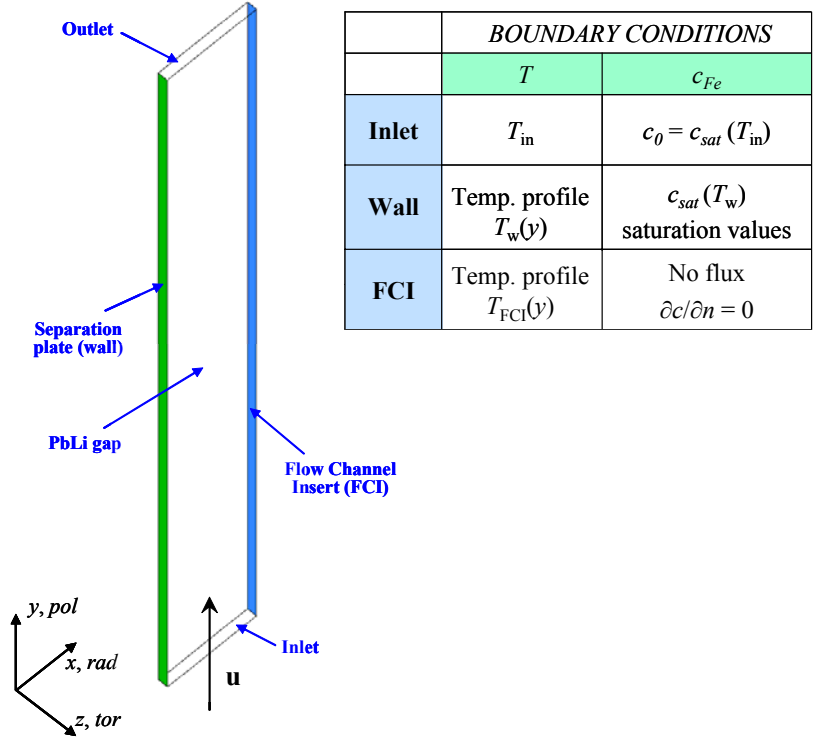


Figure 20: Sketch showing boundary conditions for the temperature T and iron concentration c_{Fe} applied in the calculations. Here c_{sat} indicates the saturation concentration, y is the poloidal coordinate and n is the transverse direction, normal to the FCI, here the radial direction x . The separation plate is simply called wall.

At the surface of the flow channel insert no flux has been assumed for the concentration. In Sect.2.3 it is shown that the temperature variation across the gap is very small. For that reason a temperature distribution equal to that at the wall-liquid metal interface has been given, i.e. $T_{FCI1}(y) \simeq T_w(y)$. Here the subscript 1 indicates the PbLi-FCI interface at the gap side and 2 will be used to denote the interface at the bulk side.

The employed fluid dynamic code CFX assumes internally a boundary condition at the outlet and a constant gradient constraint is imposed, generally different from zero.

3.2 Saturation concentration and diffusion coefficient

Long-term exposure tests carried out on specimens of the martensitic steel MANET in the PbLi loop PICOLO (Borgstedt, Drechsler, Frees and Peric (1988)) showed that for ferritic steels the corrosion, after an incubation period, needed before the samples fully interact with the liquid metal, is governed by uniform dissolution of iron and chromium (Borgstedt and Röhrig (1991)). The incubation period can be related to the presence of a passivation layer that has to be dissolved before having a complete wetting of the steel surface. The authors show that the steady state corrosion of ferritic steel in flowing PbLi alloy for temperatures in the range 500–550 °C is governed by dissolution processes. The experiments made in the PICOLO loop considered a flowing PbLi with a velocity of 0.3 m s⁻¹ in the test section. Material losses were determined by measuring both the reduction in thickness and in weight of the specimens.

Borgstedt and Röhrig (1991) derived values for the diffusivity of iron and chromium in PbLi from the ones available in Pb by introducing a correction factor given by the ratio of the PbLi viscosity and the one of Pb, $(\eta_{PbLi}/\eta_{Pb})^{-1} = 0.56$, considering the Einstein-Stokes relation that connects the diffusion coefficient D with the viscosity η ($\eta \sim T/D$). According to Robertson (1968) who describes the diffusivity D through the relation

$$D = D_0 \exp\left(-\frac{Q}{RT}\right),$$

where D_0 is a constant ($D_{0,Fe} = 4.9 \cdot 10^{-7} \text{ m}^2 \text{ s}^{-1}$), R is the gas constant $R = 8.31447 \text{ J} \cdot \text{K}^{-1} \text{ mol}^{-1}$, T is the temperature in Kelvin and $Q = 10500 \pm 1500 \text{ cal mol}^{-1}$, the iron diffusivity in lead is given by:

$$D_{Fe/Pb}(T) = 4.9 \cdot 10^{-7} \exp(-5280/T) \text{ m}^2 \text{ s}^{-1}. \quad (24)$$

By introducing the above mentioned correction factor a value $D_{Fe/PbLi}(500^\circ\text{C}) = 2.96 \cdot 10^{-10} \text{ m}^2 \text{ s}^{-1}$ for the mass diffusivity of Fe in PbLi is obtained at $T = 500^\circ\text{C}$.

In Fig.21 the mass diffusion coefficient as given by (24) for the temperature range of the problem under study is plotted as a function of the wall temperature.

Borgstedt and Röhrig (1991) and Borgstedt and Feuerstein (1992) give also an expression for the solubility of iron in PbLi, assuming that it is similar to the one in Pb given by Stevenson and Wulff (1961):

$$c_s(T) = 31.6 \exp\left(-\frac{14046}{T}\right) \quad (25)$$

or

$$\log c_s(T) = 3.5 - \frac{6100}{T}. \quad (26)$$

In the last equation the saturation concentration is expressed in mole fraction (percentage). The values obtained by this formula have been compared with the experimental data from corrosion tests in turbulent flow (Borgstedt and Feuerstein (1992)).

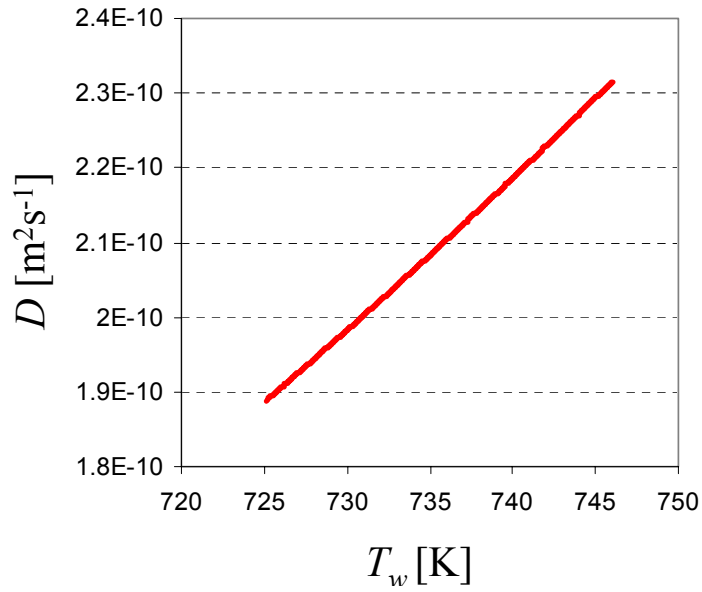


Figure 21: Mass diffusion coefficient plotted as a function of the wall temperature.

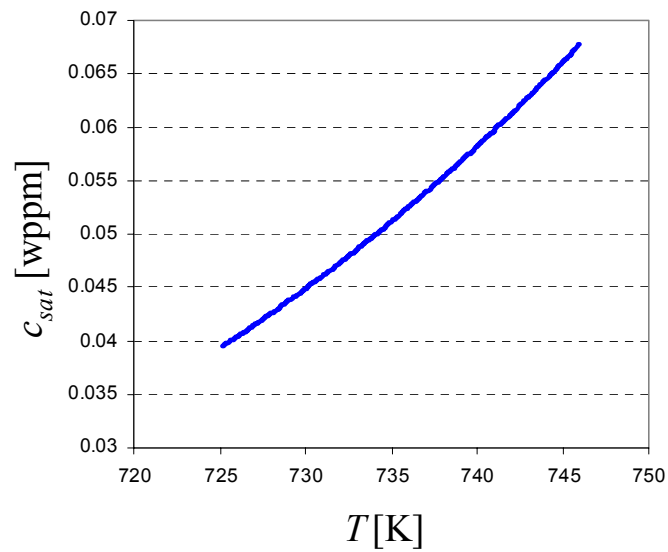


Figure 22: Saturation concentration c_{sat} of iron atoms in PbLi as a function of the temperature.

In equation (25) c_s is expressed in atomic fractions (atoms of iron/atoms of PbLi) and T is the absolute temperature. In order to convert this value of concentration in mass fraction it is necessary to multiply it by the ratio of the atomic mass of iron to the molecular weight of PbLi. The molecular weight can be calculated as the sum of the individual atomic masses of all the atoms forming the molecule. Although for an alloy the molecular weight should take into account the electronic structure of the molecule, as an approximation it has been calculated according to the common definition:

$$MW_{PbLi} = 207.2 \text{ u} \cdot 0.83 + 6.941 \text{ u} \cdot 0.17 = 173.156 \text{ u},$$

where u is called atomic mass unit.

Figure 22 shows the saturation concentration c_{sat} of iron from eq.(25) as a function of the temperature.

The validity of the described relations for the solubility and diffusion coefficients of iron in the eutectic liquid alloy PbLi is also supported by Borgstedt and Gumin-ski (2002). They show that these data are consistent with the Einstein-Sutherland equation. Moreover, the authors justify the use of solubility values similar to the ones obtained for the iron in Pb by saying that the Fe-solubility in PbLi should not be strongly affected by the presence of lithium. This is due to the fact that, since the alloy PbLi can be considered as a quasi-binary alloy of Pb-PbLi (Jauch et al. (1986)), Li interacts much more with Pb than with Fe atoms and therefore the dissolution of iron atoms by Li is unlikely.

4 Numerical model

The present problem is solved by using the commercial code CFX. Here an additional variable c is defined that describes the concentration of Fe atoms that dissolve in the liquid metal. A transport equation, which includes an advection and a diffusion term, is solved for this new variable. The concentration of iron has been defined as a specific additional variable given in terms of the amount of the conserved quantity per unit mass of fluid.

In CFX 5.6 the general form of a transport equation for additional variables is:

$$\frac{\partial c}{\partial t} + \nabla \cdot (\mathbf{v} c) = \nabla \cdot (D \nabla c)$$

where c is the conserved quantity per unit mass, D is the kinematic diffusivity for the scalar property.

The only equation solved during the run is the one for the concentration; the other variables, namely the velocity and the temperature, have been determined in advance and they stay at their imposed initial values. Fluid properties, saturation concentration and diffusion coefficient are taken with reference to the local temperature determined according to the afore-mentioned procedure (Sect.2.3).

5 Results

Results have been obtained for two different imposed velocity profiles, calculated for two values of the electrical conductivity of the flow channel insert, $\sigma_{FCI} = 500 \Omega^{-1}\text{m}^{-1}$ and $\sigma_{FCI} = 100 \Omega^{-1}\text{m}^{-1}$, as shown in Fig.10b (Sect.5.1.3). In the first case there is a higher maximum velocity. The velocity fields come from the analysis of the MHD flow in the poloidal ducts in a DCLL blanket module (Mistrangelo, Raffray and Aries Team (2007) and Part I of this report).

Figure 23 shows the concentration of iron in the gap as a function of the radial direction, namely across the width of the gap for various poloidal positions. Here, the concentration is given in mass fraction, i.e. in grams of solute per grams of fluid [g_{sol}/g_{fluid}]. A higher concentration of dissolved iron is present only in half of the gap, close to the steel wall. Figure 23a displays the results obtained considering a velocity distribution calculated for the case with $\sigma_{FCI} = 500 \Omega^{-1}\text{m}^{-1}$ and Fig.23b corresponds to $\sigma_{FCI} = 100 \Omega^{-1}\text{m}^{-1}$, namely to smaller given velocities.

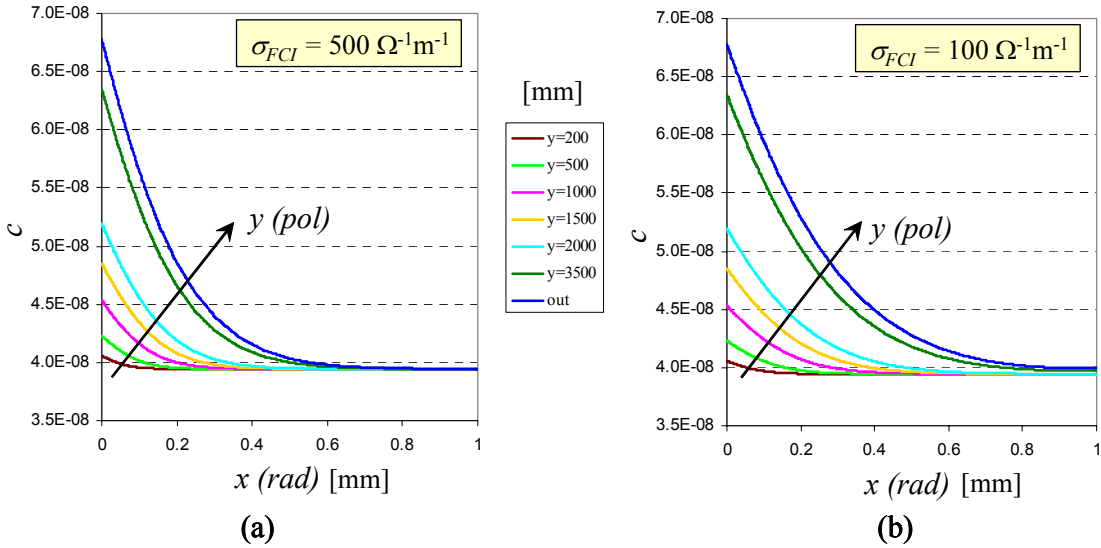


Figure 23: Concentration distribution given in grams of solute per grams of fluid (mass fraction) across the gap width, i.e. along the radial direction, at various poloidal positions. The results are obtained considering the MHD velocity profile obtained for (a) $\sigma_{FCI} = 500 \Omega^{-1}\text{m}^{-1}$ and (b) $\sigma_{FCI} = 100 \Omega^{-1}\text{m}^{-1}$.

We observe that at a fixed radial position, namely at a given distance from the wall, the concentration of iron increases towards the exit of the duct. This is due to the fact that the atoms of iron that dissolve in the liquid metal in the gap are then transported by convection towards the exit of the channel. Moreover, this is related to the assumption that at the wall the concentration reaches the saturation value that increases with the temperature. This effect can be seen also in Fig.24 where the iron concentration is plotted as a function of the poloidal direction for several radial locations.

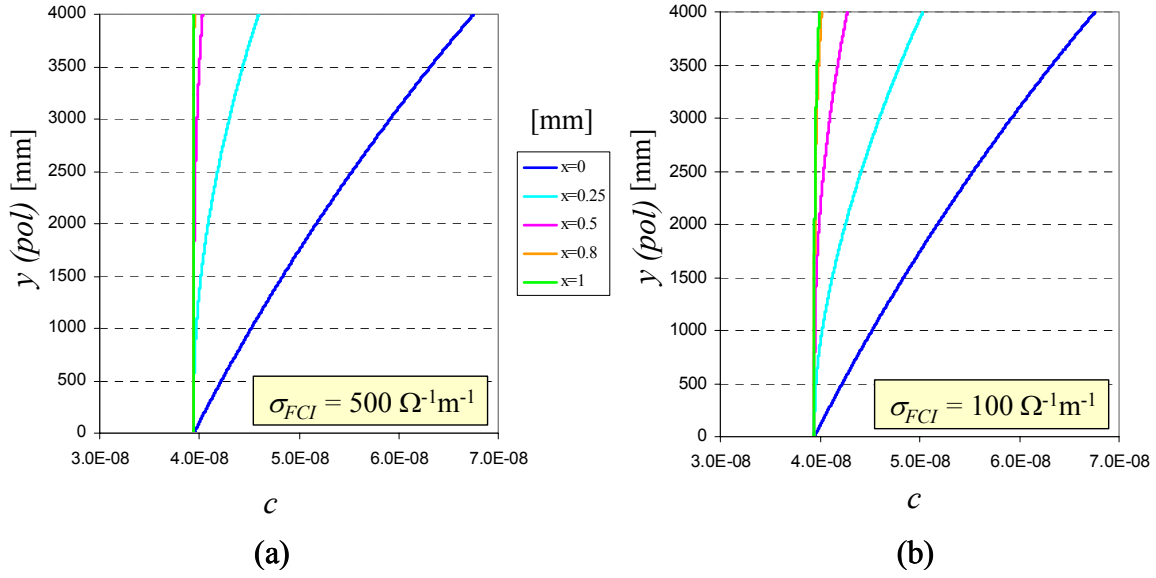


Figure 24: Concentration of iron (mass fraction) along the poloidal direction, at various radial positions. The steel wall is located at $x = 0$ and the FCI at $x = 1$ mm. The results are obtained imposing the MHD velocity profile calculated for the case with (a) $\sigma_{FCI} = 500 \Omega^{-1} \text{m}^{-1}$ and (b) $\sigma_{FCI} = 100 \Omega^{-1} \text{m}^{-1}$.

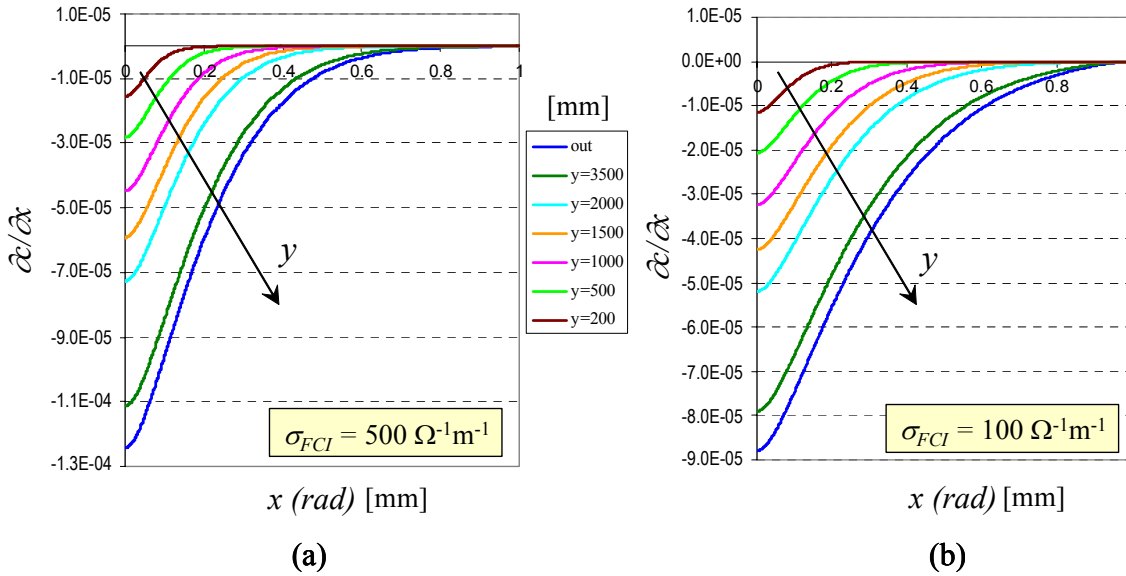


Figure 25: Gradient of iron concentration in direction perpendicular to the wall plotted along the radial direction, at various poloidal positions. The results are obtained considering the MHD velocity profile calculated for (a) $\sigma_{FCI} = 500 \Omega^{-1} \text{m}^{-1}$ and (b) $\sigma_{FCI} = 100 \Omega^{-1} \text{m}^{-1}$.

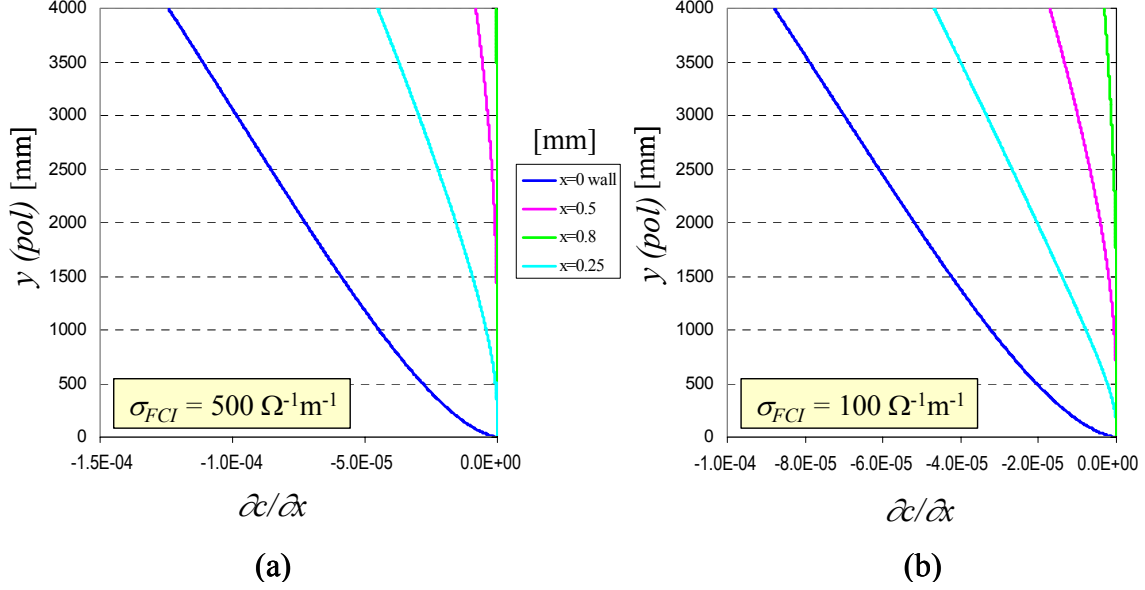


Figure 26: Gradient of iron concentration in direction perpendicular to the wall, along the poloidal direction for several radial locations across the gap width. Results are obtained considering the MHD velocity profile computed for (a) $\sigma_{FCI} = 500 \Omega^{-1}\text{m}^{-1}$ and (b) $\sigma_{FCI} = 100 \Omega^{-1}\text{m}^{-1}$.

By comparing the results obtained imposing two different velocity profiles we notice that, in the case of larger electrical conductivity of the insert, when the velocity is higher, the concentration at a selected position in the gap is smaller due to the stronger advection.

The concentration gradient in direction perpendicular to the wall, i.e. the mass flux that enters the fluid from the wall, increases along the poloidal direction as shown in Figs.25-26. When the imposed velocity is larger ($\sigma_{FCI} = 500 \Omega^{-1}\text{m}^{-1}$) the gradient, namely the corrosion rate, is higher than for lower velocity ($\sigma_{FCI} = 100 \Omega^{-1}\text{m}^{-1}$)

The corrosion rate is given by the product of the concentration gradient normal to the wall ($\partial c/\partial x$) and the mass diffusion coefficient (D). Since the concentration is expressed in mass fraction, it is necessary to multiply the obtained quantity by the ratio of the PbLi density ($\rho_{PbLi} = 9.5 \text{ g cm}^{-3}$) to that of iron ($\rho_{Fe} = 7.87 \text{ g cm}^{-3}$). It is obtained that at the outlet the corrosion rate is of the order of $1 \mu\text{m}/\text{year}$. This value is smaller than the ones found in the literature (Bucenieks, Krishbergs, Platacis, Lipsbergs, Shishko, Zik and Muktupavela (2005)). This can be related to the assumption that the concentration at the entrance is equal to the saturation value at the inlet temperature. The experiments performed at the University of Latvia instead are obtained using a purified liquid metal at the inlet, obtained by installing in the loop a cold trap to remove the dissolved corrosion products. Moreover, the reference temperature in their experiments was higher ($T = 550 \text{ }^\circ\text{C}$). We can also notice that many experiments have been performed under turbulent flow conditions and instead in the calculations a laminar fully developed MHD profile is assumed.

6 Conclusions

Calculations have been performed to analyze the mass transfer problem of corrosion products in flowing PbLi in the gaps formed between the flow channel inserts and the steel walls in the poloidal ducts that transport the liquid metal in a DCLL blanket module. This study has the purpose to give a first assessment of the importance of corrosion of the steel wall in a DCLL blanket. Uncertainties are still present concerning the saturation concentration and mass diffusivity values used in the numerical analysis. The large scattering among the available experimental data and the fact that often they do not cover the needed temperature range and flow conditions, requires still a careful evaluation of the selected formulas. Moreover, there is often a large difference between the flow conditions assumed in the numerical analysis and those used in the experiments. For that reason further investigations are required to refine these first results. Ongoing discussions and simulations will give a more complete and reliable picture of the importance of corrosion in the proposed blanket concept for ARIES-CS.

From the first analysis it seems that, due to the small velocities in the gaps formed between the flow channel inserts and the walls, these latter will not suffer from a strong and critical corrosion. A corrosion rate of the order of $1 \mu\text{m}/\text{year}$ has been found. Nevertheless, it is important to remark that some assumptions have been considered that may lead to an underestimation of the corrosion rate. In particular, one important reason for this low corrosion rate can be identified in the assumed saturation of the PbLi imposed at the inlet of the poloidal ducts. This could be an indication that the entire liquid metal loop have to be modelled in order to obtain the correct balance between corrosion and deposition processes. Therefore, a realistic quantitative estimation of the corrosion rate requires a dedicated model for the mass transfer of wall material into the fluid. This model should take into account local interface temperature and the possible under-saturation of the PbLi with iron and chromium at the duct entrance. Chromium has been omitted in the analysis due to the strong uncertainties over the data for diffusion coefficient and saturation values.

7 Future investigations

In order to understand the effect of the assumptions under which the problem has been studied, other calculations will be carried out for instance considering a different temperature range and other initial conditions for the concentration assuming $c_{in} < c_{sat}(T_{in})$. Moreover, in this first investigation the properties of steel (e.g. the heat transfer coefficient) have been considered constant, but a dependence on the temperature could be included.

Results in the literature (Borgstedt and Feuerstein (1992)) show that due to the presence of lithium the solubility of some metals in the eutectic PbLi alloy could increase compared to that in pure lead. Therefore, further studies are foreseen by using different values of the iron solubility.

References

- Borgstedt, H., Drechsler, G., Frees, G. and Peric, Z.: 1988, Corrosion testing of steel x 18 CrMoVNb 12 1 (1.4914) in a Pb-17Li pumped loop, *Journal of Nuclear Materials* **155-157**, 728–731.
- Borgstedt, H. and Feuerstein, H.: 1992, The Solubility of Metals in Pb-17Li Liquid Alloy, *Journal of Nuclear Materials* **191-194**, 988–991.
- Borgstedt, H. and Guminski, C.: 2002, A model for the prediction of the corrosion of steels in flowing liquid lead alloys, *Journal of Nuclear Materials* **303**, 240–241.
- Borgstedt, H. U. and Röhrig, H. D.: 1991, Recent Results on Corrosion Behaviour of MANET Structural Steel in Flowing Pb-17Li Eutectic, *Journal of Nuclear Materials* **197-181**, 596–598.
- Broc, M., Flament, T., Fauvet, P. and Sannier, J.: 1988, Corrosion of austenitic and martensitic stainless steels in flowing 17Li—83Pb alloy, *Journal of Nuclear Materials* **155-157(2)**, 710–714.
- Buceniaks, I., Krishbergs, R., Platacis, E., Lipsbergs, G., Shishko, A., Zik, A. and Muktupavela, F.: 2005, Investigation of corrosion effects of EUROFER steel in Pb-17Li stationary flow in the magnetic field, *Proceedings of the 15th Riga and 6th PAMIR Conference on Fundamental and Applied MHD, June 27-July 1, Riga, Jurmala, Latvia* **1**, 255–258.
- Bühler, L. and Molokov, S.: 1994, Magnetohydrodynamic flows in ducts with insulating coatings, *Magnetohydrodynamics* **30(4)**, 439–447.
- Flament, T., Tortorelli, P., Coen, V. and Borgstedt, H.: 1992, Compatibility of materials in fusion first wall and blanket structures cooled by liquid metals, *Journal of Nuclear Materials* **191-194**, 132–138.
- He, X., Li, N. and Mineev, M.: 2001, A kinetic model for corrosion and precipitation in non-isothermal LBE flow loop, *Journal of Nuclear Materials* **297(2)**, 214–219.
- Jauch, U., Karcher, V., Schulz, B. and Haase, G.: 1986, Thermophysical properties in the system Li-Pb, *Report KfK 4144*, Kernforschungszentrum Karlsruhe.
- Malang, S.: 1984, Influence of a magnetic field on liquid metal corrosion, *Fusion Technology 1984, Proceedings of the 13th Symposium on Fusion Technology, Varese, Italy, 24-28 September 1984*, Pergamon Press, pp. 1424–1428.
- Malang, S., Bojarsky, E., Bühler, L., Deckers, H., Fischer, U., Norajitra, P. and Reiser, H.: 1993, Dual coolant liquid metal breeder blanket, in C. Ferro, M. Gasparotto and H. Knoepfel (eds), *Fusion Technology 1992, Proceedings of the 17th Symposium on Fusion Technology, Rome, Italy, 14-18 September 1992*, Elsevier, pp. 1424–1428.

- Malang, S. and Tillack, M. S.: 1995, Development of self-cooled liquid metal breeder blankets, *Report FZKA 5581*, Forschungszentrum Karlsruhe.
- McCarthy, K. A. and Abdou, M. A.: 1991, Analysis of liquid metal MHD flow in multiple adjacent ducts using an iterative method to solve the core flow equations, *Fusion Engineering and Design* **13**, 363–380.
- Mistrangelo, C.: 2005, Three-dimensional MHD flow in sudden expansions, *Report FZKA 7201*, Forschungszentrum Karlsruhe. PhD Thesis, University of Karlsruhe.
- Mistrangelo, C., Raffray, A. R. and Aries Team: 2007, MHD Analysis of Dual Coolant Pb-17Li Blanket for ARIES-CS, *Fusion Science and Technology* **52**(4), 849–854.
- Molokov, S.: 1993, Fully developed liquid-metal flow in multiple rectangular ducts in a strong uniform magnetic field, *European Journal of Mechanics, B/Fluids* **12**(6), 769–787.
- Morley, N. B., Malang, S. and Kirillov, I.: 2005, Thermofluid magnetohydrodynamic issues for liquid breeders, *Fusion Science and Technology* **47**(3), 488–501.
- Müller, U. and Bühler, L.: 2001, *Magneto-fluid dynamics in Channels and Containers*, Springer, Wien, New York. ISBN 3-540-41253-0.
- Najmabadi, F. and Raffray, A. R.: 2006, Recent progress in the ARIES compact stellarator study Fusion Engineering and Design, *Fusion Engineering and Design* **81**(23-24), 2679–2693.
- Najmabadi, F., Raffray, R., Ku, L. P., Lyon, J. F. and the ARIES Team: 2006, Optimization of compact stellarator configuration as fusion devices, *Physics of Plasmas* **13**, 056123–1.
- Najmabadi, F. and the ARIES Team: 2007, Final report of ARIES-CS study. It will be published as a special issue of Fusion Science and Technology. Preprints available at <http://aries.ucsd.edu/ARIES/>.
- Patankar, S. V.: 1980, *Numerical Heat Transfer and Fluid Flow*, Hemisphere.
- Raffray, A. R., El-Guebaly, L., Ihli, T., Malang, S., Najmabadi, F., Wang, X. and the ARIES-CS Team: 2007, Engineering challenges in designing an attractive compact stellarator power plant, *Fusion Engineering and Design* **82**, 2696–2704.
- Robertson, W.: 1968, *Trans. Met. Soc. AIME* **242**, 2139.
- Rome (Editor), J. A.: 1998, U.S. Stellarator Program Plan, *Stellarator News* **57**, 4–6.
- Sannier, J., Flamment, T. and Terlain, A.: 1991, Corrosion of martensitic steel in flowing Pb17Li, *Fusion Technology 1990*, Esevier, pp. 881–885.
- Shercliff, J. A.: 1965, *A Textbook of Magnetohydrodynamics*, Pergamon Press, Oxford.

- Smolentsev, S., Morley, N. B. and Abdou, M.: 2006, Magnetohydrodynamic and thermal issues of the SiCf/SiC flow channel insert, *Fusion Science and Technology* **50**(1), 107–119.
- Stevenson, D. and Wulff, J.: 1961, Liquid-solid phase distribution studies in the systems iron-lead, cobalt-lead, chromium-tin, and nickel-silver, *Trans. Met. Soc. AIME* **221**, 271–275.
- Tillack, M. S. and Malang, S.: 1997, High Performance PbLi Blanket, *Proceedings of the 17th IEEE/NPSS Symposium Fusion Engineering, San Diego, California October 6-10*, Vol. 2, Institute of Electrical and Electronics Engineers, Inc., pp. 1000–1004.
- Walker, J. S.: 1986, Liquid metal flow through a thin walled elbow in a plane perpendicular to a uniform magnetic field, *Int. J. Engng. Sci.* **24**(11), 1741–1754.